Another look at stochastic condensation for subgrid cloud modeling: adiabatic evolution and effects

Christopher A. Jeffery *
Space and Remote Sensing Sciences (ISR-2), LANL, Los Alamos, NM

Jon M. Reisner & Miroslaw Andrejczuk
Atmospheric, Climate and Environmental Dynamics (EES-2), LANL, Los Alamos, NM

Manuscript: JAS-2147

September 13, 2006

Abstract

The theory of stochastic condensation, which models the impact of an ensemble of unresolved supersaturation fluctuations S' on the volume-averaged droplet-size distribution $f(r)$, is revisited in the modern context of subgrid cloud parameterization. The exact transition probability density for droplet radius driven by independent, Gaussian S' fluctuations that are periodically renewed is derived and shown to be continuous but not smooth. The Fokker-Planck model follows naturally as the smooth-in-time approximation to this discrete-in-time process. Evolution equations for the moments of $f(r)$ that include a contribution from subgrid S' fluctuations are presented; these new terms are easily implemented in moment-based cloud schemes that resolve supersaturation. New, self-consistent expressions for the evolution of $f(r)$ and mean-supersaturation $\overline{S}$ in a closed, adiabatic volume are derived without approximation; quite appropriately, these coupled equations exactly conserve total water mass. The behavior of this adiabatic system, which serves as a surrogate for a closed model grid column, is analyzed in detail. In particular, a new non-dimensional number is derived that determines the relative impact of S' fluctuations on droplet spectral evolution, and the contribution of fluctuations to $\overline{S}$ is shown to be negative definite, maximal near the accommodation length and has a direct correspondence to the analysis of Cooper (1989). Observational support for the theory of stochastic condensation is found in cloud droplet spectra from cumulus cloud fields measured during the RICO and SCMS campaigns. Increasing spectral broadening with increasing spatial scale is discovered and compares well with theoretical predictions. However, the observed spectra show evidence of non-Gaussian S' fluctuations and inhomogeneous mixing, processes neglected in the current theory.

*Corresponding author address: Christopher A. Jeffery, Los Alamos National Laboratory (ISR-2), PO Box 1663, Mail Stop D-436, Los Alamos, NM 87545, USA. Tel.: (505) 665-9169; fax: (505) 664-0362. Email: cjeffery@lanl.gov

1. Introduction

One of the most important theoretical constructs in atmospheric science is the gradient transport model for the flux $\overline{\boldsymbol{u}'\zeta'}$,

$$\overline{\boldsymbol{u}'\zeta'} = -K\boldsymbol{\nabla}\overline{\zeta} \tag{1}$$

which enables the derivation of logarithmic profiles of mean horizontal velocity ($\zeta' = u'$) and temperature ($\zeta' = T'$) in the atmospheric surface layer and provides a subgrid closure (eddy viscosity and diffusivity) for atmospheric models. In modern atmospheric texts and treatments, the gradient model is usually postulated a priori. But underlying this model is a rich stochastic framework that, in the earlier years of atmospheric science, was given due consideration. The interested reader is referred to Sutton (1953) for the historical flavor of this discussion.

In fact, the origin of the gradient transport model is found in Fokker-Planck theory developed to describe the evolution of the distribution function of a system of microscopic entities that obey a stochastic Lagrangian evolution equation called the Langevin equation (Risken 1989). The Langevin equation un-

derlying Eq. (1) is simply

$$\frac{\mathrm{d}\boldsymbol{X}}{\mathrm{d}t} = \boldsymbol{u}'$$

where $\boldsymbol{X}$ is the Lagrangian position of a fluid ($\zeta' = u'$) or scalar ($\zeta' = T'$) element and $\boldsymbol{u}'$ is an independently specified random variable with de-correlation time, τ. Seen in this light, the gradient model approximation is analogous to the Fokker-Planck approximation that truncates the Kramers-Moyal expansion to 1st order in τ (Risken 1989).

The truncation that gives the Fokker-Planck equation is valid for system evolution times $t \gg \tau$, regardless of the distribution of $\boldsymbol{u}'$. For molecular diffusion of gases in air, τ is on the order of picoseconds and thus $t \gg \tau$ is clearly satisfied for all atmospheric applications. However, in the case of unresolved turbulent transport, τ is given by the grid-cell large-eddy turn-over time and the condition $t \gg \tau$ is not necessarily satisfied. In this case, the validity of the Fokker-Planck or gradient model depends on the distribution of $\boldsymbol{u}'$, with good model accuracy obtained if $\boldsymbol{u}'$ is normally distributed as is often observed in the atmosphere.

It is natural, then, to inquire whether this stochastic formulation may have applicability in other subgrid problems. In the 1960s a group of Russian scientists (Belyaev 1961; Sedunov 1965; Mazin 1965; Levin and Sedunov 1966a,b) investigated the evolution of the droplet-size distribution, $f(r)$, by postulating a stochastic component to droplet growth

$$\frac{\mathrm{d}r}{\mathrm{d}t} \sim \frac{S'}{r+a}$$

where r is droplet radius, a is an accommodation length often set to zero, and S' is a random supersaturation fluctuation with the correlation $\overline{S'f'}$ analogous to the flux $\overline{\boldsymbol{u}'\zeta'}$. Appropriately, this theoretical approach has inherited the name "stochastic condensation", and it has largely garnered interest as a potential mechanism for spectral broadening to large droplet sizes. Despite the obvious analogy to the ubiquitous eddy-diffusivity parameterization, the investigation of the correlation $\overline{S'f'}$ and its corresponding gradient model, has largely been ignored outside of the Russian community with few exceptions (e.g. Manton (1979); Khvorostyanov and Curry (1999a,b)). Very recently, Mcgraw and Liu (2006) analyzed the steady-state behavior of $f(r)$ within the context of Fokker-Planck theory.

In this work we take another look at the theory of stochastic condensation with the overarching goals of (i) clarifying earlier derivations and presenting new exact results, (ii) motivating the use of stochastic condensation as a subgrid cloud model by assessing the impact of S'-fluctuations on a closed, adiabatic volume, and (iii) using in-situ observations of droplet spectra averaged over a fixed segment length to provide parameter estimates for subgrid cloud modeling. These goals are achieved in the following specific ways. In Sec. 2 we introduce a stochastic model that assumes S' is independently and normally distributed with given time-dependent variance, $\sigma^2(t)$ and fixed renewal time. The assumption that S' is explicitly Gaussian differs from the approach of the early Russian investigators but is advantageous for two important reasons:

- As a point of consistency, the assumption $t \gg \tau$ is not necessary and the application of stochastic condensation to subgrid modeling is appropriate.
- The present Gaussian model is exactly solvable. The availability of an exact solution for $f(r)$ has application outside of this work (Andrejczuk et al. 2006).

It should be further emphasized that we do not construct a model for $\sigma^2(t)$, nor do we relate S' to vertical velocity; rather, we treat $\sigma^2(t)$ as externally provided. A discussion of the validity of these modeling assumptions is postponed until their consequences have been deduced.

Having derived the exact analytic solution to the present model in Sec. 3, and the corresponding Fokker-Planck equation in Sec. 4, the rest of the article pertains to the evolution of $f(r)$ in a closed, adiabatic volume. As discussed by Merkulovich and Stepanov (1981) among others, the equations for temperature and total parcel liquid water content (or equivalently mean parcel supersaturation, $\overline{S}$) are coupled to $f(r)$ and must be considered. We derive this analytic coupling without approximation in Sec. 5, and the coupled evolution of $\{\overline{S}, f\}$ in a closed, adiabatic volume is assessed—both with (Sec. 5) and without (Sec. 6) recourse to the quasi-stationary assumption. The objective of this analysis is to quantify the impact of unresolved Gaussian supersaturation fluctuations on a closed, adiabatic volume as a function of relevant non-dimensional numbers, and thereby, motivate the use of stochastic condensation as a subgrid cloud model. Finally, we assess the length dependence of segment averaged cloud droplet spectra from cumulus fields in Sec. 7 and use the comparison of modeled and observed spectra to provide estimates of the relevant parameters for subgrid modeling purposes. Sec. 8 contains a summary.

2. The Model

Following the proceeding discussion, we introduce the following exactly solvable model of stochastic condensation and evaporation. The supersaturation field along the i-th droplet's trajectory is decomposed into mean, $\overline{S}(t)$, and fluctuating, $S'(i,t)$, components where S' is a centered, independent random variable that obeys a Gaussian law and is renewed after a time, $\tau(t)$. This renewal process imparts a discrete nature on the droplet statistics. Let us decompose continuous time, t, into segments of length τ:

$$t = \sum_{i=1}^{n-1} \tau_i + \varphi\tau_n \tag{2}$$

where the restriction $\varphi \in [0,1)$ uniquely defines the integer n for a given t. The label n thereby denotes the time interval $\sum_{i=1}^{n-1}\tau_i \le t < \sum_{i=1}^{n}\tau_i$ and the corresponding supersaturation S'_n drawn at time $t = \sum_{i=1}^{n-1}\tau_i$ from a Gaussian of variance σ_n^2. With this notation, the two-time statistics of S' are given by

$$\langle S'_m(i,t_1)S'_n(j,t_2)\rangle = \sigma_n^2\delta_{mn}\delta_{ij} \tag{3}$$

where $\langle\cdot\rangle$ represents an ensemble average over S'. To complete the model we specify the following Langevin equation:

$$\dot{r} = \frac{\alpha(\overline{S}+S')}{r+a} \tag{4}$$

where $a \approx 2\ \mu\mathrm{m}$ is an accommodation length and α is defined in Appendix A.

A key underlying assumption of the present model is that τ is independent of the radius r_i of the i-th droplet. This assumption is inherent to much of the work on stochastic condensation although it is rarely discussed†. Statistical independence of τ and r_i is justified at large spatial scales (many cubic meters in extent) where each coherent S'-region contains a full ensemble of droplet sizes. Thus each ensemble of droplets of a given size—scattered densely throughout the volume—evolve according to the given system evolution time τ. Recently, Jeffery and Reisner (2006) investigated the de-correlation time of S during the mixing of clear and cloudy air and found that $\tau = \max(\tau_{\mathrm{react}}, \tau_{\mathrm{eddy}})$ where τ_{eddy} is the system (grid-cell) large-eddy turn-over time and τ_{react} is the phase relaxation time (Squires 1952). It must be emphasized that within the context of the present model, τ can be any time-dependent arbitrary function of the moments of r.

† Khvorostyanov and Curry (1999a) offers an effort to relax this assumption.

A few words on the specification of $\overline{S}$ are in order. Since the early studies of Levin and Sedunov (1966a,b, 1967), $\overline{S}(t)$ has typically been given as a constant, externally specified parameter. In the present context of subgrid cloud parameterization, this approach is insufficient because it does not ensure conservation of water mass and entropy within the grid cell or column (Merkulovich and Stepanov 1981). Consistent with an Eulerian model, we define $\overline{S}$ as the spatially averaged supersaturation in a volume of air that evolves according to (Pruppacher and Klett 1997, pp. 513)

$$\frac{\mathrm{d}\overline{S}}{\mathrm{d}t} = A_1\overline{w} - A_2\overline{\frac{\rho_l}{dt}}$$

where $\{A,B\}$ are constants, w is vertical velocity, ρ_l is liquid water density and an overbar represents a spatial average. Following standard methods, we then evoke the ergodic hypothesis which equates this spatial average with an ensemble average over all droplet radii and supersaturations:

$$\frac{\mathrm{d}\overline{S}}{\mathrm{d}t} = \frac{\mathrm{d}}{\mathrm{d}t}\left\langle\langle S\rangle_r\right\rangle = A_1\overline{w} - A_2\frac{\mathrm{d}}{\mathrm{d}t}\left\langle\langle\rho_l\rangle_r\right\rangle$$

where $\langle\cdot\rangle_r$ represents an ensemble average over r. The ergodic hypothesis demands that the droplets in every range $[r, r+dr]$ experience a complete ensemble of S'. The validity of this assumption improves with increasing volume size; at a minimum, we require a volume of several cubic meters in extent. It must be emphasized that knowledge of the individual distributions of r and S' is insufficient to evaluate the double average $\langle\langle\cdot\rangle_r\rangle$ since r and S' are not independent. Rather, the joint r-S' distribution function is needed.

Within the context of subgrid cloud modeling at coarse resolution, the present model provides no information on the number, location or spatial structure of the modeled clouds. Thus the physical interpretation of the present model is relatively unconstrained. Consider, for example, the case where a significant fraction of the support of $f(r)$ resides on $r \le 0$, i.e. a significant fraction of droplets have evaporated completely. We may infer this to be the outcome of a single entrainment event in an updraft, or the death of several cumuli in a cloud field containing many clouds. In the same manner, not all clouds modeled by the present approach need be of the same age—a collection of droplets that grow stochastically from zero size at a given time may represent the growth of a new cloud†. This is both the strength and weak-

† For this scenario, more accurate results are obtained by including droplet activation.

ness of subgrid ensemble modeling—no spatial information is needed, but unfortunately, the subgrid spatial structure is indeterminate.

3. Exact Analytic Solution

We proceed to calculate the exact transition probability distribution function for a *single* droplet, $G(r,t|r_0)$. This derivation exploits the seminal property that the sum of two independent Gaussian random variables is, itself, a Gaussian random variable. Integrating Eq. (4) gives

$$(r+a)^2 = (r_0+a)^2 + 2\alpha\int_0^t \mathrm{d}\xi\ \overline{S}(\xi) + 2\alpha\lambda(t) \quad (5)$$

where

$$\lambda \equiv \int_0^t \mathrm{d}\xi\ S'(\xi)$$

and $r(t=0)=r_0$. It is important to emphasize that Eq. (5) does not incorporate a boundary condition at $r=0$ that prevents the prediction of negative radii. Thus this equation is only valid for those S' fluctuations that give $r \geq 0$. In terms of G, this restriction demands $G=0$ for $r<0$.

The discrete nature of S' appears in the evaluation of λ for the present model:

$$\lambda(t) = \sum_{i=1}^{n-1}\tau_i S_i' + \varphi\tau_n S_n'. \quad (6)$$

Since the sum of independent Gaussian random variables is Gaussian, it follows immediately that λ is normally distributed with variance $\sum_{i=1}^{n-1}\tau_i^2\sigma_i^2 + \varphi^2\tau_n^2\sigma_n^2$. A more rigorous derivation of this result formally convolves over all $\{S_1', S_2', \ldots, S_n'\}$ combinations that produce a given λ. For example, denoting the first term on the rhs of Eq. (6) λ_0, the probability of λ is

$$P(\lambda) = \langle P(\lambda_0)P(S')\rangle_{\lambda_0+\varphi\tau_n S'=\lambda}$$

where the condition $\lambda_0 + \varphi\tau_n S' = \lambda$ selects the relevant subset of all $\{\lambda_0, S'\}$ combinations. Computing this expected value we find

$$\begin{aligned} P(\lambda) &= \int_{-\infty}^{\infty}\mathrm{d}S' \frac{1}{\sqrt{2\pi\sum_{i=1}^{n-1}\tau_i^2\sigma_i^2}}\exp\left[-\frac{(\lambda-\varphi\tau_n S')^2}{2\sum_{i=1}^{n-1}\tau_i^2\sigma_i^2}\right] \\ &\quad \frac{1}{\sqrt{2\pi}\sigma_n}\exp\left(-\frac{S'^2}{2\sigma_n^2}\right) \\ &= \frac{\exp\left[-\frac{\lambda^2}{2(\sum_{i=1}^{n-1}\tau_i^2\sigma_i^2+\varphi^2\tau_n^2\sigma_n^2)}\right]}{\sqrt{2\pi(\sum_{i=1}^{n-1}\tau_i^2\sigma_i^2+\varphi^2\tau_n^2\sigma_n^2)}} \end{aligned} \quad (7)$$

which is a Gaussian with variance $\sum_{i=1}^{n-1}\tau_i^2\sigma_i^2 + \varphi^2\tau_n^2\sigma_n^2$, as expected.

Using Eq. (5) and the relation, $P(r) = (\partial\lambda/\partial r)P(\lambda)$, gives

$$G(r,t|r_0) = \frac{r+a}{\sqrt{\pi\mathcal{D}_{\mathrm{int}}}}\exp\left(-\frac{\Delta^2}{4\mathcal{D}_{\mathrm{int}}}\right) \quad (8)$$

with time-integrated diffusivity

$$\mathcal{D}_{\mathrm{int}}(t) \equiv 2\alpha^2\left(\sum_{i=1}^{n-1}\tau_i^2\sigma_i^2 + \varphi^2\tau_n^2\sigma_n^2\right) \quad (9)$$

and where

$$\Delta \equiv (r+a)^2 - (r_0+a)^2 - 2\alpha\int_0^t \mathrm{d}\xi\overline{S}(\xi)$$

is the difference between $(r+a)^2$ and the value obtained from evolving $(r_0+a)^2$ in time using the mean supersaturation $\overline{S}$. Taking the limit of vanishing S'-fluctuations, $\sigma^2 \to 0$, we find that G converges to a delta-function giving $\Delta \to 0$, as expected.

Equation (8) is the exact analytic solution to the model of Sec. 2. We reiterate that this solution is strictly valid when $G(r<0)=0$. However, as long as the solution for $r>0$ retains its full skewed-Gaussian form, i.e. $\lim_{r\to 0} G \ll a(\pi\mathcal{D}_{\mathrm{int}})^{-1/2}$, neglect of the $r=0$ boundary condition in the derivation of the analytic solution is justified. In practice, this limits the applicability of the present model to those $\{r_0, \overline{S}(t), \mathcal{D}_{\mathrm{int}}(t)\}$ which keep the support of G away from $r=0$. The discrete nature of the renewal process is evident in the definition of $\mathcal{D}_{\mathrm{int}}$. While the variance of S' may vary continuously in time, the renewal process samples S' at discrete times $t \in \{0, \tau, 2\tau, \ldots, (n-1)\tau\}$.

3a. *Time-independent* σ^2

The connection between Eq. (8) and a diffusive process with diffusivity $\mathcal{D}$ is revealed when the statistics of S' are time-independent. In this case, Eq. (8) becomes

$$G(r,t|r_0) = \frac{r+a}{\sqrt{\pi\mathcal{D}\gamma}}\exp\left(-\frac{\Delta^2}{4\mathcal{D}\gamma}\right) \quad (10)$$

where $\mathcal{D} \equiv 2\tau\alpha^2\sigma^2$ and the time

$$\gamma(t) = \{(n-1)+\varphi^2\}\tau \quad (11)$$

where $\{\varphi, n\}$ are defined implicitly by Eq. (2). Equation (10) has the familiar form of a Green's function solution describing the r-space diffusion of $(r+a)^2$. As expected, $\mathcal{D}$ exhibits a linear dependence on the renewal time, τ, and the S' variance, σ^2.

Inspection of Eqs. (2) and (11) reveals that γ differs from t; this comparison is shown in Fig. 1. The two times agree periodically at every $\varphi = 0$, while at $\varphi = 1/2$, t exceeds γ by $\tau/4$. While γ is continuous in time it is not smooth, and all the statistics of spectral evolution inherit this lack of smoothness.

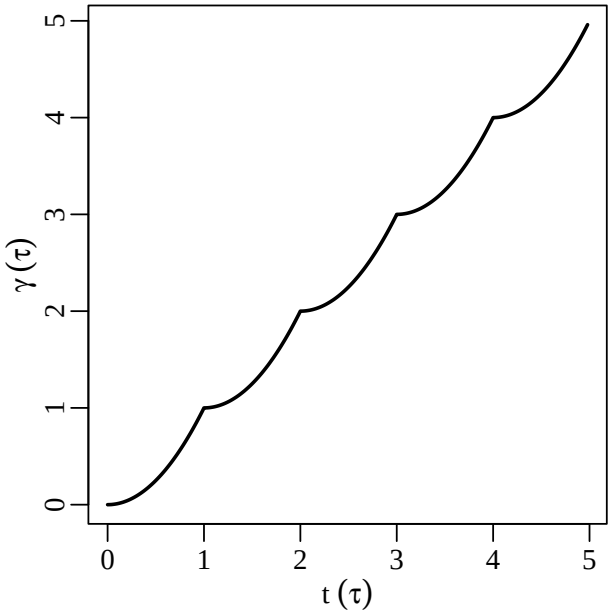

Figure 1: The function $\gamma(t)$, defined by Eq. (11), is continuous but not smooth, and is periodically equal to t when S' is renewed ($\varphi = 0$).

3b. *Droplet population*

For a population of droplets where the S' renewal times are *synchronized*, i.e. all droplet S'-renewals occur at the same time, the droplet-size probability density function, $f(r,t)$, is given by the convolution of G with the initial distribution of sizes, $f_0(r)$:

$$f(r,t) = \int_0^\infty \mathrm{d}r_0 \; f_0(r_0) G(r,t|r_0)$$

The present model is of sufficient generality to incorporate distributions of renewal times that are not synchronized. A pertinent example is the case where the renewal time, τ, is the same for each drop but the first renewal event differs and occurs at a time $\varphi_0\tau$ with $\varphi_0 \in [0,1]$. Evaluation of f now includes a convolution over the initial distribution, $\varphi(\varphi_0)$, of φ_0 values:

$$f(r,t) = \int_{-\infty}^\infty \mathrm{d}r_0 \int_0^1 \mathrm{d}\varphi_0 \; f_0(r_0)\varphi(\varphi_0) G(r,t|r_0,\varphi_0)$$

3c. $\langle S'|r\rangle$ *and the PDF equation*

The exact analytic solution $G(r,t|r_0)$ has a corresponding equation that is formed by spatially averaging the general PDF equation for $\tilde{f}(r,t,\boldsymbol{x})$ over a droplet field where $\tilde{r}(t,\boldsymbol{x})$ is the radius of the droplet at $(t,\boldsymbol{x})$ and $\tilde{f} \equiv \delta(r-\tilde{r}(t,\boldsymbol{x}))$ is the single-point density function. In the present context, this spatial average is replaced by an ensemble average over S', such that $f(r,t) = \langle f(r,t,S')\rangle$ where $f(r,S')$ is the joint $\{r,S'\}$ distribution function. The general PDF equation in this case is

$$\frac{\partial f(r,t)}{\partial t} = -\frac{\partial}{\partial r}\left(\left\langle \frac{\mathrm{d}r}{\mathrm{d}t} f(r,t,S')\right\rangle\right)$$

which, for the present model, is conveniently written in terms of the conditional quantity $\langle S'|r\rangle$ (Jeffery and Reisner 2006):

$$\frac{\partial f(r,t)}{\partial t} = -\alpha\overline{S}\frac{\partial}{\partial r}\left(\frac{f(r,t)}{r+a}\right) - \alpha\frac{\partial}{\partial r}\left(\frac{\langle S'|r\rangle}{r+a} f(r,t)\right) \tag{12}$$

The quantity $\langle S'|r\rangle$ is the expected value of S' for each r and it facilitates the formulation of a PDF equation for the single unknown $f(r,t)$. We calculate $\langle S'|r\rangle$ below for the present model with constant $\{\sigma^2,\tau\}$, synchronized S' fluctuations and for the transition probability $f(r,t) = G(r,t|r_0)$. These restrictions on the statistics of S' are not fundamental and are only imposed to simplify notation.

By definition, $\langle S'|r\rangle$ depends on $f(r,t,S')$ and is therefore an implicit function of f_0:

$$\langle S',t|r\rangle \equiv \int_{-\infty}^\infty \mathrm{d}S' \; S' f(S',t|r)$$

where Bayes theorem states that $f(S'|r) \equiv f(r,S')/f(r)$. These relations imply that we **cannot** calculate $\langle S'|r\rangle$ once for $f(r) = G(r|r_0)$ and then convolve over various f_0 afterwards.

Construction of the joint-distribution function $f(r,S')$ for the present model begins with Eq. (7) for $P(\lambda)$. We first note that for the special case $f(r) = G(r|r_0)$

$$\langle S',t|r\rangle_G = \int_{-\infty}^\infty \mathrm{d}S' \; S' G(S',t|r,r_0) \tag{13}$$

where the subscript G emphasizes that the statistic $\langle\cdot\rangle$ holds only for $f = G$. Returning to the integrand

of Eq. (7), substituting for λ, and using the simplification of constant $\{\sigma^2, \tau\}$ gives

$$G(r, S', t|r_0) = \frac{r+a}{\sqrt{\pi\mathcal{D}}(t-\varphi\tau)^{1/2}} \exp\left\{-\frac{(\Delta - 2\alpha S'\varphi\tau)^2}{4\mathcal{D}(t-\varphi\tau)}\right\} \frac{1}{\sqrt{2\pi}\sigma} \exp\left(-\frac{S'^2}{2\sigma^2}\right)$$

Dividing $G(r, S')$ by Eq. (10) for $G(r)$ gives

$$G(S', t|r, r_0) = \frac{1}{\sqrt{2\pi}\sigma}\left\{\frac{\gamma}{(t-\varphi\tau)}\right\}^{1/2} \exp\left\{-\gamma\frac{\left(S' - \frac{\varphi}{2\alpha\gamma}\Delta\right)^2}{2(t-\varphi\tau)\sigma^2}\right\} \quad (14)$$

This equation preserves an important property of the renewal process, namely, that the statistics of S' are independent of r at the moment, $\varphi = 0$, when S' is sampled. For $\varphi \neq 0$, "unusually" large drops where $\Delta \gg 0$ are associated with positive S', while $\Delta \ll 0$ corresponds to negative S'. For bounded Δ we also observe that

$$\lim_{t\to\infty} G(S', t|r, r_0) = P(S', t)$$

This limiting behavior expresses the intuitive statement that as droplets sample more and more S' realizations, their radii become increasingly statistically independent of the current S'.

Using Eqs. (13) and (14) we finally arrive at

$$\langle S', t|r\rangle_G = \frac{\varphi}{2\alpha\gamma}\Delta \quad (15)$$

which is discontinuous in time and expresses that $\langle S'|r\rangle_G = 0$ at the moment, $\varphi = 0$, when S' is sampled, $\langle S'|r\rangle_G \sim \Delta$ otherwise, and

$$\lim_{t\to\infty} \langle S', t|r\rangle_G = 0$$

for bounded Δ. Closing Eq. (12) using (15) we find that, indeed, $G(r)$ given by Eq. (10) is a solution of the resulting equation†.

The conditional quantity, $\langle S'|r\rangle_G$, determines the net r-space "velocity", v_G, caused by the S' fluctuations as seen from Eq. (12).

$$v_G \equiv \frac{\alpha\langle S'|r\rangle_G}{r+a} = \frac{\varphi}{2\gamma}\frac{\Delta}{(r+a)}.$$

This velocity is positive (negative) for $\Delta > 0$ ($\Delta < 0$) and causes G to broaden about $\Delta = 0$.

† Note that the relation $\partial/\partial t = 2\varphi\partial/\partial\gamma$ is helpful in this regard.

4. Fokker-Planck Approximation

The only difference between the behavior of the exact transition distribution function, Eq. (8), for the present model and r-space diffusion of $(r+a)^2$ with a time-dependent diffusivity is the discrete nature of $\mathcal{D}_{\rm int}$ which is exemplified in the behavior of γ shown in Fig. 1. Replacing the discrete, φ^2-weighted sampling of σ^2 by its continuous surrogate gives the Fokker-Planck approximation to the exact solution.

The Fokker-Planck equation describing the evolution of the PDF of $\beta = (r+a)^2$ with drift $2\alpha\overline{S}$ and diffusivity $\mathcal{D}_{\rm FP}$ is

$$\frac{\partial f_{\rm FP}(\beta, t)}{\partial t} = -2\alpha\overline{S}\frac{\partial f_{\rm FP}}{\partial\beta} + \mathcal{D}_{\rm FP}\frac{\partial^2 f_{\rm FP}}{\partial\beta^2}$$

where $\mathcal{D}_{\rm FP}(t) \equiv 2\tau\alpha^2\sigma^2$ is the continuous version of Eq. (9). Straightforward manipulation yields

$$\frac{\partial f_{\rm FP}(r,t)}{\partial t} = -\alpha\overline{S}\frac{\partial}{\partial r}\left(\frac{f_{\rm FP}}{r+a}\right) + \frac{\mathcal{D}_{\rm FP}}{4}\frac{\partial}{\partial r}\frac{1}{(r+a)}\frac{\partial}{\partial r}\frac{f_{\rm FP}}{(r+a)} \quad (16)$$

with Green's function solution

$$G_{\rm FP}(r, t|r_0) = \frac{r+a}{\sqrt{\pi\int_0^t \mathrm{d}\xi\mathcal{D}_{\rm FP}(\xi)}} \exp\left(-\frac{\Delta^2}{4\int_0^t \mathrm{d}\xi\mathcal{D}_{\rm FP}(\xi)}\right) \quad (17)$$

Equations (16) and (17), unlike the exact solution, are smooth. We observe that $G_{\rm FP}$ is equal to G at the renewal times $t = i\tau$. Formally we can derive $G_{\rm FP}$ from G by taking the limit $\tau \to 0$ while holding $\mathcal{D}_{\rm int}$ constant. This renormalization is an approximation that holds when $\tau \ll t$ for all t of interest. The small τ limit does not generally hold for turbulent systems where τ corresponds to the system (grid cell) large-eddy turnover time.

Equations (16) and (17) were first derived by Belyaev (1961) and further explored by Sedunov (1965) and Levin and Sedunov (1966a,b, 1967) for $a = 0$. These authors *do not* derive an exact solution and then infer the Fokker-Planck equivalent as we have done here. Rather they use standard methods from Fokker-Planck theory that are available in many texts, e.g. Risken (1989), and are not pursued here. Of further interest, Manton (1979) uses a first order smoothing approximation to derive Eq. (16) from correlated S' fluctuations and the $\tau \to 0$ renormalization.

A comparison of G and $G_{\rm FP}$ for $t \in \{3, 3.5, 4\}\tau$, $\overline{S} = 0$, constant $\{\sigma^2, \tau\}$, $r_0/a = 5$ and $r_0^4/(\mathcal{D}\tau) = 30$ is shown in Fig. 2. For visual clarity, $\{G, G_{\rm FP}\}$ is translated to the right for successive times. Also shown is the histogram, $G_{\rm sim}$, obtained from a

stochastic simulation of 10^7 droplets. Good agreement is seen between G and $G_{\rm sim}$ demonstrating that with 10^7 droplets—still 10^4–10^7 less than a typical model grid-cell—the stochastic simulation has converged to the ensemble result. The figure also shows that at $t = 3.5\tau$ ($\varphi = 0.5$), the Fokker-Planck approximation **overestimates** the distribution width as compared to the ensemble and stochastic results. This overestimation scales with t/γ, and decreases with increasing t. These graphical results demonstrate that, while G is the appropriate solution to assess the accuracy of stochastic droplet models (Andrejczuk et al. 2006), $G_{\rm FP}$ is of sufficient accuracy for atmospheric modeling applications.

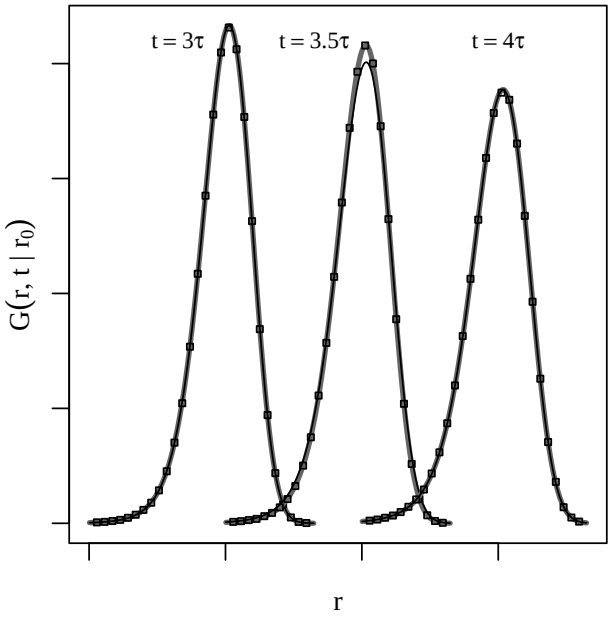

Figure 2: Comparison at $t \in \{3, 3.5, 4\}\tau$ of the exact ensemble result G (thick gray line; Eq. (10)) with the Fokker-Planck approximation $G_{\rm FP}$ (thin black line; Eq. (17)) and the histogram $G_{\rm sim}$ (□), computed from a stochastic simulation of 10^7 droplets. Distributions are shown for $0 \le r \le 1.65 r_0$ and are translated to the right at successive times for visual clarity. Parameter values are $\overline{S} = 0$, constant $\{\sigma^2, \tau\}$, $r_0/a = 5$ and $r_0^4/(\mathcal{D}\tau) = 30$.

4a. $\langle S'|r\rangle_{\rm FP}$

Comparison of Eqs. (12) and (16) gives the expression for $\langle S'|r\rangle$ in the Fokker-Planck approximation:

$$\langle S'|r\rangle_{\rm FP} = -\frac{\mathcal{D}_{\rm FP}}{4\alpha}\frac{1}{f_{\rm FP}}\frac{\partial}{\partial r}\left\{\frac{f_{\rm FP}}{(r+a)}\right\} \qquad (18)$$

This expression is of greater generality than Eq. (15) for $\langle S'|r\rangle_G$ derived in Sec. 3c because it is valid for any $f_{\rm FP}$. For the special case $f_{\rm FP}$ = $G_{\rm FP}$ and constant $\{\sigma^2, \tau\}$, Eq. (18) gives

$$\langle S'|r\rangle_{{\rm FP},G} = \frac{\Delta}{4\alpha t} \qquad (19)$$

which can be compared to the exact result, (15). This comparison reveals that the Fokker-Planck approximation in this case is equivalent to transforming $\gamma \to t$ and replacing $\varphi(t)$ by its average value of 1/2. Thus $\langle S'|r\rangle_{{\rm FP},G}$ is the natural continuous approximation to the discontinuous behavior of $\langle S'|r\rangle_G$.

4b. *Moments*

Equations for the evolution of the r-moments can be used to incorporate unresolved supersaturation fluctuations into cloud schemes that resolve $\overline{S}$ but do not use bin microphysics. Using the definition $\langle\cdot\rangle_r \equiv \int_0^\infty {\rm d}r\ \cdot$, Eq. (16) and assuming all moments exist, integration by parts gives the following equations for the evolution of the r-moments:

$$\begin{aligned}
\frac{{\rm d}\langle r\rangle_r}{{\rm d}t} &= \alpha\overline{S}\left\langle\frac{1}{r+a}\right\rangle_r - \frac{\mathcal{D}_{\rm FP}}{4}\left\{\frac{f_{\rm FP}(0,t)}{a^2} + \left\langle(r+a)^{-3}\right\rangle_r\right\} \\
\frac{{\rm d}\langle r^2\rangle_r}{{\rm d}t} &= 2\alpha\overline{S}\left\langle\frac{r}{r+a}\right\rangle_r + \frac{\mathcal{D}_{\rm FP}}{2}\left\langle\frac{a}{(r+a)^3}\right\rangle_r \\
\frac{{\rm d}\langle r^3\rangle_r}{{\rm d}t} &= 3\alpha\overline{S}\left\langle\frac{r^2}{r+a}\right\rangle_r + \frac{3\mathcal{D}_{\rm FP}}{4}\left\langle\frac{r(r+2a)}{(r+a)^3}\right\rangle_r
\end{aligned} \qquad (20)$$

valid for $a > 0$. These equations reveal that the impact of S'-fluctuations on the evolution of the first three moments depends strongly on f in the "small r" region $r \le a$. In particular, for narrow spectral support, $\overline{S} > 0$ and fixed $\{\overline{S}, \mathcal{D}_{\rm FP}\}$, the $\overline{S}$-term increasingly dominates the diffusion term as the spectrum grows to larger sizes.

5. Adiabatic evolution and effects

The goal of this section is to determine how the incorporation of unresolved supersaturation fluctuations—as modeled by either Eq. (16) or (20)—into an $\overline{S}$-resolving cloud microphysical scheme will impact $\overline{S}$ and the moments of $f(r)$. The early studies of stochastic condensation and evaporation neglected the impact of S' on the adiabatic evolution

of $\overline{S}$, e.g. (Levin and Sedunov 1966a,b, 1967). The first self-consistent derivation of evolution equations for both $\overline{S}$ and f in terms of a single diffusivity, $\mathcal{D}_{\rm FP}$, was performed by Voloshchuk and Sedunov (1977). Quite surprisingly, Voloshchuk and Sedunov use the r-evolution equation, which does not express conservation of mass and entropy, to arrive at the correct (adiabatic) expression for $\overline{S}$. But, as we shall see, a first-order Taylor series approximation lead Voloshchuk and Sedunov, by chance, to the exact result.

5a. $\sigma^2 = 0$

We first consider the evolution of $\overline{S}$ of a closed adiabatic volume (grid-cell) with a non-disperse population of droplets of size r_0 at $t = 0$; this analysis lays the foundation for the $\sigma^2 \neq 0$ case considered subsequently. For this study, we ignore the dependence of droplet activation on supersaturation and assume that the system contains a given number of droplets at $t = 0$. This is a classical problem in cloud physics that has been studied since the 1950s.

The equation for $\overline{S}$ for the present scenario is

$$\frac{{\rm d}\overline{S}}{{\rm d}t} = c_1\overline{w}(t) - c_2\frac{{\rm d}r^3}{{\rm d}t} \tag{21}$$

where c_1 and c_2 are defined in Appendix A. Using the well-known quasi-stationary (QS) assumption, $d\overline{S}/dt = 0$ in Eq. (21), corresponding to the low-frequency behavior of $\overline{S}(t)$, and integrating Eq. (21) gives

$$r^3 = r_0^3 + a^3 N_z(t)$$

where

$$N_z(t) \equiv \frac{c_1}{c_2 a^3} z(t)$$

and $z(t) = \int_0^t {\rm d}\xi\ \overline{w}(\xi)$. The non-dimensional number N_z determines the linear relationship between liquid water and height $z(t)$, and the r-moments are given by $r^n = (r_0^3 + a^3 N_z)^{n/3}$.

Using Eq. (5) and substituting $\mathcal{B}_{\rm QS} = \beta^2/a^2$ with $\beta = (r_0 + a)^2 + 2\alpha \int_0^t {\rm d}\xi\ \overline{S}(\xi)$ gives

$$\left(\mathcal{B}_{\rm QS}^{1/2} - 1\right)^3 = \frac{r_0^3}{a^3} + N_z(t) \tag{22}$$

such that $\overline{S}_{\rm QS} = a^2/(2\alpha) d\mathcal{B}_{\rm QS}/dt$ and where a subscript QS refers to a quantity evaluated using the quasi-stationary assumption.

5b. $\sigma^2 \neq 0$

We now consider the evolution of $\overline{S}$ of a closed, adiabatic volume with S' fluctuations using the model of Sec. 2. Invoking the ergodic hypothesis, the evolution equation for $\overline{S}$ is a function of the joint r-S' statistics:

$$\begin{aligned}
\frac{{\rm d}\overline{S}}{{\rm d}t} &= c_1\overline{w}(t) - c_2\left\langle\left\langle\frac{{\rm d}r^3}{{\rm d}t}\right\rangle_r\right\rangle \\
&= c_1\overline{w}(t) - 3\alpha c_2\left\{\left\langle\frac{r^2}{r+a}\right\rangle_r \overline{S} + \left\langle\left\langle\frac{r^2}{r+a}\middle| S'\right\rangle_r S'\right\rangle\right\} \quad (23a)\\
&= c_1\overline{w}(t) - 3\alpha c_2\left\{\left\langle\frac{r^2}{r+a}\right\rangle_r \overline{S} + \left\langle\frac{r^2}{r+a}\langle S'|r\rangle\right\rangle_r\right\} \quad (23b)
\end{aligned}$$

It is important to emphasize that there are two distinct averaging procedures that appear in Eq. (23): the $\langle\cdot\rangle$ average over an ensemble of S' fluctuations and the $\langle\cdot\rangle_r$ average over $f(r)$. The only difference between Eqs. (23a) and (23b) is the order in which the averaging is performed. We have already discussed the conditional average $\langle S'|r\rangle$ in some detail and will proceed to evaluate Eq. (23b) using the Fokker-Planck approximation.

Substitution of the Fokker-Planck expression, $\langle S'|r\rangle_{\rm FP}$, into Eq.(23b) and integration by parts gives

$$\frac{{\rm d}\overline{S}_{\rm FP}}{{\rm d}t} = c_1\overline{w}(t) - 3\alpha c_2\left\{\left\langle\frac{r^2}{r+a}\right\rangle_r \overline{S}_{\rm FP} + \frac{\mathcal{D}_{\rm FP}}{4\alpha}\left\langle\frac{r(r+2a)}{(r+a)^3}\right\rangle_r\right\} \tag{24}$$

valid for $a > 0$. Eqs. (16) and (24) form two coupled, self-consistent equations that describe the evolution of $\{f_{\rm FP}, \overline{S}_{\rm FP}\}$ in a closed, adiabatic system. As a consistency check we note that the new (3rd) term on the rhs of Eq. (24) could have also been derived by simply substituting Eq. (20) for $d\left\langle r^3\right\rangle_r/dt$ directly into $d\overline{S}_{\rm FP}/dt = c_1\overline{w} - c_2 d\left\langle r^3\right\rangle_r/dt$. Clearly, Eqs. (16) and (24) conserve total water.

For $a = 0$, the integration by parts produces a boundary term so that Eq. (24) is more conveniently written

$$\frac{{\rm d}\overline{S}_{\rm FP}}{{\rm d}t} = c_1\overline{w}(t) - 3\alpha c_2\left\{\langle r\rangle_r \overline{S}_{\rm FP} - \frac{\mathcal{D}_{\rm FP}}{4\alpha}F_*\right\}$$

where $F_* = \int_0^\infty {\rm d}r\ r\partial/\partial r(f/r)$. The quasi-stationary (QS) evaluation of $\overline{S}_{\rm FP}$ is

$$\overline{S}_{\rm FP,QS} = \frac{c_1\overline{w}(t)}{3\alpha c_2\langle r\rangle_r} + \frac{\mathcal{D}_{\rm FP}}{4\alpha}\frac{F_*}{\langle r\rangle_r} \tag{25}$$

which is a result first derived by Voloshchuk and Sedunov (1977) using equations that do not express conservation of mass and entropy [†]. Voloshchuk

[†]The corresponding F_* term in Voloshchuk and Sedunov is diffi cult to fi nd; it is the 2nd term on the 2nd line of their Eq. (25). A more explicit representation of this result is the 1st term on the 2nd line of Eq. (2.13) in Smirnov and Nadeykina (1986) where $\widetilde{A}_1$ must be interpreted as an operator acting on (D_e/r).

and Sedunov obtain the exact, adiabatic result by chance—their first order Taylor series expansion of $(\langle r\rangle_r + \langle r\rangle_r')^{-1}$ in the r-evolution equation happens to give the same correction to $\langle r\rangle_r\,\overline{w}$ that appears in the $\overline{S}$ equation, properly averaged. The same Taylor series expansion of $(\langle r\rangle_r + \langle r\rangle_r')^{-1}$ is also used by Cooper (1989, Eq. (7)).

Finally, we note that Mcgraw and Liu (2006) recently derive an expression for $\overline{S}_{\rm FP}$ using the steady-state solution (Weibull distribution) to the Fokker-Planck equation. It is straightforward to show that the Mcgraw and Liu result is a special case of Eq. (25) that holds when $\overline{w} = 0$ and f is time-independent.

5c. $\overline{S}_{\rm FP,QS}$

The QS evaluation of $\overline{S}_{\rm FP}$ from Eq. (24) is

$$\overline{S}_{\rm FP,QS} = \frac{c_1\overline{w}(t)}{3\alpha c_2}\left\langle\frac{r^2}{r+a}\right\rangle_r^{-1}\left\{1 - \frac{\mathcal{D}_{\rm FP}}{4}\frac{3c_2}{c_1\overline{w}(t)}\langle J\rangle_r\right\} \tag{26}$$

valid for $a > 0$ where $J = r(r+2a)/(r+a)^3$. This result shows that the presence of S'-fluctuations in a closed cell—as prescribed by the present model—act to decrease $\overline{S}_{\rm FP}$. In the language of Cooper (1989, pp. 1306), this occurs because high-$\langle r\rangle_r$ regions tend to have $S' > 0$ and low-$\langle r\rangle_r$ regions have $S' < 0$. However, we emphasize that smaller $\overline{S}_{\rm QS}$ values do not imply a trend toward evaporation. In fact, Eq. (23) demonstrates that grid-averaged liquid water density is proportional to $\overline{w}(t)$ and independent of S' in the QS limit.

The impact of S'-fluctuations on $\overline{S}_{\rm FP,QS}$ depends on $f_{\rm FP}$ via the spectral moment $\langle J\rangle_r$. A plot of $\langle J\rangle_r$ vs $\langle r\rangle_r$ is shown in Fig. 3 for three different $f_{\rm FP}$. The figure demonstrates that $\langle J\rangle_r$ peaks in the vicinity of $\langle r\rangle_r = a$ where a is typically around 2 μm. This result reiterates the conclusion of Sec. 4b that the parameterization of unresolved S' variability in a numerical model will have the greatest impact on smaller droplet sizes.

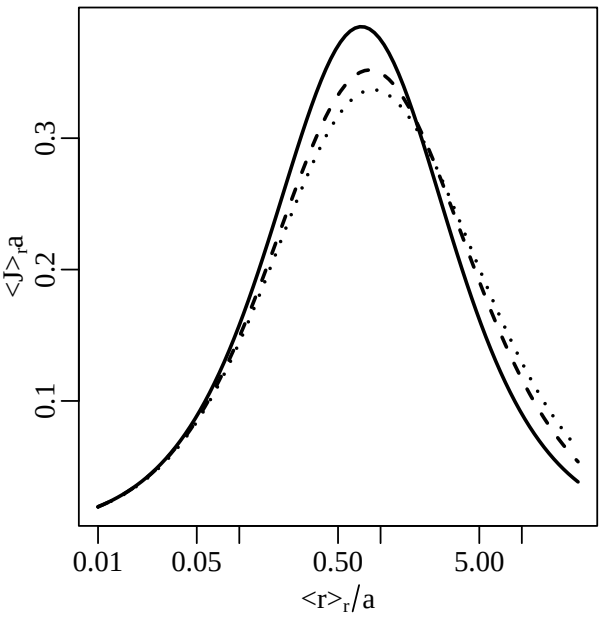

Figure 3: Comparison of $\langle J\rangle_r$ as a function of $\langle r\rangle_r$ computed from three distributions: the gamma function $f_{\rm FP} \sim r^n e^{-(n+1)r/\langle r\rangle_r}$ with $n = 1$ ($\cdots$) and $n = 2$ (- -), and a non-disperse spectrum $f_{\rm FP} = \delta(r - \langle r\rangle_r)$ corresponding to the limit $n \to \infty$ (—). $\langle J\rangle_r$ peaks in the vicinity of $\langle r\rangle_r = a$ for all three $f_{\rm FP}$.

5d. *Non-dimensional number,* $N_{\mathcal{D}}$

In Sec. 5a, the usefulness of the non-dimensional number N_z for the case $\sigma^2 = 0$ was highlighted. For $\sigma^2 \neq 0$, we can construct a 2nd non-dimensional number that determines the relative impact of S'-fluctuations on $\mathcal{B}_{\rm QS}$ and hence the r-moments.

In appendix B we derive the non-dimensional number

$$N_{\mathcal{D}}(t) \equiv \frac{c_2}{c_1}\frac{\int_0^t {\rm d}\xi\ \mathcal{D}_{\rm FP}(\xi)}{az(t)} \tag{27}$$

The number $N_{\mathcal{D}}$ is thus the ratio of two time-integrated forcing terms in the $\overline{S}_{\rm FP}$ evolution equation—diffusion ($c_2\mathcal{D}_{\rm FP}/a$) and velocity ($c_1\overline{w}$)—and, as Eq. (30) reveals, $N_{\mathcal{D}}$ determines the relative impact of S'-fluctuations on $\mathcal{B}_{\rm QS}$. Note that when both $\{\overline{w}, \mathcal{D}_{\rm FP}\}$ are constant, $N_{\mathcal{D}} = c_2\mathcal{D}_{\rm FP}/(c_1 a\overline{w})$ is also constant.

$N_{\mathcal{D}}$ increases with increasing $\mathcal{D}_{\rm FP}$ as expected, but it also decreases with increasing $\overline{w}$, in agreement with concerns raised by Manton (1979, pp. 902) that large updraft velocities decrease the relative importance of S'-fluctuations. Formally, $N_{\mathcal{D}} \sim z^{-1}(t)$; a similar algebraic dependence is found in the results of Cooper (1989, Eq. (10)) in his evaluation of a turbulent correction to $\mathcal{B}_{\rm QS}$. However, the additional dependence $N_{\mathcal{D}} \sim a^{-1}$ is, perhaps, surprising and indicates the importance of regularizing the growth law $dr/dt \sim r^{-1}$ in the limit $r \to 0$.

5e. *Impact of* $N_{\mathcal{D}}$ *on* $\overline{S}_{\rm FP}$

Using the QS approximation, the coupled behavior of $\{\overline{S}_{\rm FP}, f_{\rm FP}\}$ can be solved exactly for $f_{\rm FP} = G_{\rm FP}$ ignoring boundary effects. For this scenario, an analytic expression for $\langle r^3\rangle_r$ is derived in Appendix C

such that $\beta_{\rm QS}$ is defined implicitly by the relation

$$\left\langle r^3 \right\rangle_r = r_0^3 + a^3 N_z(t) \tag{28}$$

for a given $\{N_z, N_{\mathcal{D}}\}$. Note that the behavior of $\beta_{\rm QS}$ is of relevance because there is a one-to-one correspondence between the sign of $d\beta_{\rm QS}/dN_z$ and the sign of $\overline{S}_{\rm FP}$.

A contour plot of $\mathcal{B}_{\rm QS}$ as a function of $\{N_z, N_{\mathcal{D}}\}$ calculated from Eq. (28) is shown in Fig. 4(a) for $r_0 = 0$ and $f_{\rm FP} = G_{\rm FP}$ using the analytic expression for $\left\langle r^3 \right\rangle_r$ given in Appendix C. Since $N_z \sim z(t)$ it is useful to note that the time-scale $c_2 a^3/(c_1 \overline{w})$ is of order 1 second for typical atmospheric temperatures, droplet concentrations and updraft velocities. Thus the abscissa of Fig. 4 maps closely to time in seconds for constant $\overline{w}$.

For $N_{\mathcal{D}} = 0$, $\mathcal{B}_{\rm QS}$ increases monotonically with increasing N_z as shown in the bottom of Fig. 4(a) and as indicated by Eq. (22). The figure also shows that $\mathcal{B}_{\rm QS}$ decreases with increasing $N_{\mathcal{D}}$ at fixed N_z; this result is consistent with Eq. (30). In addition, the figure indicates a shaded region where $d\mathcal{B}_{\rm QS}/dN_z < 0$ and, consequently, $\overline{S}_{\rm FP,G} < 0$. The "triple-point" that marks the beginning of this negative $\overline{S}_{\rm FP,G}$ region is $\{N_{\mathcal{D}} \approx 6.5, N_z \approx 0.15, \mathcal{B}_{\rm QS} \approx 1.5\}$. Thus the possibility of negative $\overline{S}_{\rm FP,G}$ in a closed, adiabatic updraft with internal S' fluctuations which was suggested by Eq. (26) is verified for $f_{\rm FP} = G_{\rm FP}$ in Fig. 4(a). Also shown in the figure are three dashed lines that represent predicted distributions where the fraction of droplets with $r \geq 0$ is in the set $\{0.7, 0.8, 0.9\}$. These lines divide the figure into two qualitative regimes: the upper-right region where the boundary condition imposed at $r = 0$ may impact $\mathcal{B}_{\rm QS}$ and the remaining region where this boundary-condition has little impact. The lines suggest that the prediction of negative $\overline{S}_{\rm FP,G}$ is insensitive to this bc for $N_z < 0.15$.

5f. *Impact of $N_{\mathcal{D}}$ on $r_{\rm eff}$*

We have observed a new effect of the theory of stochastic condensation which only appears when the $\overline{S}_{\rm FP}$ equation is correctly averaged and liquid water mass is exactly conserved. Namely, in a closed, adiabatic system, $\left\langle r^2 \right\rangle_r$ decreases with increasing $N_{\mathcal{D}}$ at fixed $r_{\rm vol}$. The significance of this observation is that $\left\langle r^2 \right\rangle_r$ is proportional to the short-wave scattering coefficient. Thus stochastic condensation provides a mechanism for decreasing grid-averaged cloud short-wave reflectivity while keeping cloud amount unchanged. We emphasize, however, that the droplet coalescence process may act to mitigate this effect.

A contour plot of $r_{\rm eff}/a$ with effective radius $r_{\rm eff} \equiv \left\langle r^3 \right\rangle_r / \left\langle r^2 \right\rangle_r$ is shown in Fig. 4(b) where the shaded $\overline{S}_{\rm FP,G} < 0$ region and dashed lines are again shown. In contrast to $\mathcal{B}_{\rm QS}$, $r_{\rm eff}/a$ exhibits a monotonic dependence on $\{N_z, N_{\mathcal{D}}\}$ for the shown parameter regime: $r_{\rm eff}/a$ increases with increasing N_z and increases with increasing $N_{\mathcal{D}}$. Note that no change in the trend of $r_{\rm eff}/a$ is observed in the region where $\overline{S}_{\rm FP,G} < 0$.

5g. *Summary*

Building on the pioneering work of Voloshchuk and Sedunov (1977), we consider the impact of S'-fluctuations, as prescribed by the model of Sec. 2, on the evolution of a closed, adiabatic grid-cell. This problem lends itself to non-dimensional analysis and to the identification of a finite set of time-dependent non-dimensional numbers that specify the coupled evolution of $\{f_{\rm FP}, \overline{S}_{\rm FP}\}$. Since it is the time integral of $\overline{S}_{\rm FP}$, and not $\overline{S}_{\rm FP}$ itself, that controls the evolution of $f_{\rm FP}$, we identify the set of numbers that determine the evolution of $\{f_{\rm FP}, \mathcal{B}_{\rm QS} \sim \int_0^t {\rm d}\xi\, \overline{S}_{\rm FP}(\xi)\}$ and those that diagnose $\overline{S}_{\rm FP}$, separately. This is shown in Table 1 for $f_{\rm FP} = G_{\rm FP}$ and the QS limit. Of particular importance is the number $N_{\mathcal{D}}$, Eq. (27), which controls the impact of S'-fluctuations on the evolution of $\{G_{\rm FP}, \mathcal{B}_{\rm QS}\}$.

	$G_{\rm FP}(r, t, \mathcal{B}_{\rm QS} \vert r_0)$	$\overline{S}_{\rm FP,QS}$
$\mathcal{D}_{\rm FP} = 0$	N_z	N_w
$\mathcal{D}_{\rm FP} \neq 0$	N_z, $N_{\mathcal{D}}$	N_w, $N_{\mathcal{D},\overline{S}}$

Table 1: Enumeration of the time-dependent non-dimensional numbers that determine $\{G_{\rm FP}, \mathcal{B}_{\rm QS}\}$ in the QS limit, and those that, subsequently, diagnose $\overline{S}_{\rm FP,QS}$. The numbers N_w, $N_{\mathcal{D}}$ and $N_{\mathcal{D},\overline{S}}$ are derived in appendix B. Note that $N_{\mathcal{D},\overline{S}}$ is not relevant when both $\{\mathcal{D}_{\rm FP}, \overline{w}\}$ are constant.

The range of $N_{\mathcal{D}}$ for typical atmospheric conditions and model grid scales is difficult to ascertain because the magnitude and parametric dependencies of the S'-variance, σ^2, are not well understood, and $N_{\mathcal{D}}$, itself, is time-dependent. Passive scalar theory suggests $\sigma^2 \sim L^{2/3}$ in the inertial-convective subrange where L is the grid-cell length, but this estimate is questionable since condensation damps large positive S' fluctuations. Here we choose to estimate $N_{\mathcal{D}}$ assuming time-independent $\{\overline{w}, \mathcal{D}_{\rm FP}\}$ and $\sigma = 0.01$, independent of L, while we retain Kolmogorov scaling for the renewal time, $\tau = 0.1\varepsilon^{-1/3} L^{2/3}$, where ε is the kinetic energy dissipation rate. Two contour plots of $N_{\mathcal{D}}$ are shown in

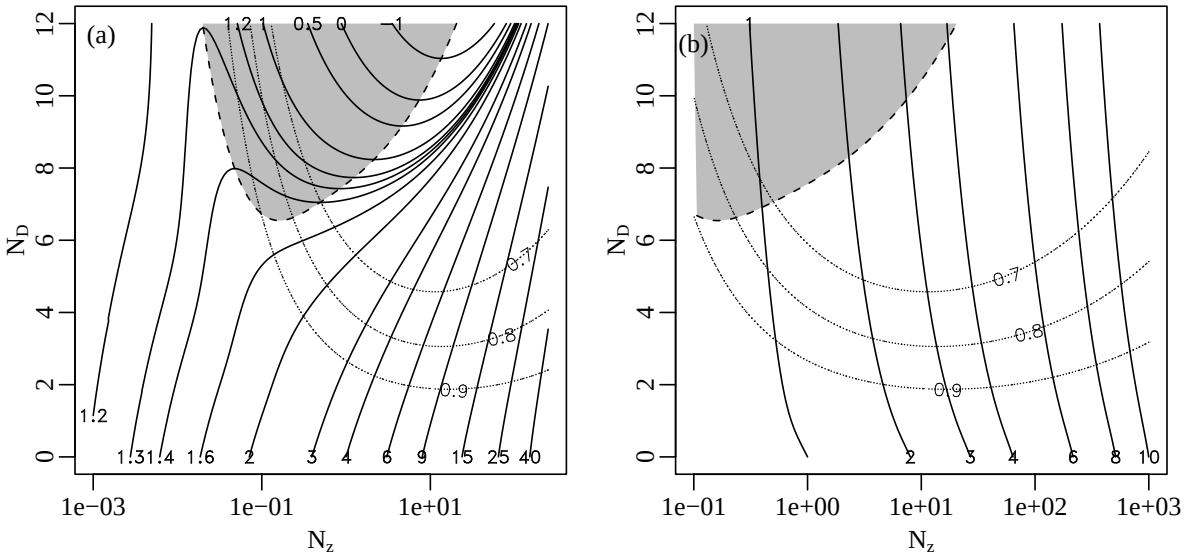

Figure 4: Contour plots of $\mathcal{B}_{\rm QS}$ [4(a)] and $r_{\rm eff}/a$ [4(b)] as a function of $\{N_z, N_{\mathcal{D}}\}$ calculated from Eqs. (28) and (31) with $r_0 = 0$, and indicated by the solid lines. The region where $d\mathcal{B}_{\rm QS}/dN_z < 0$ and, consequently, $\overline{S}_{\rm FP,G} < 0$ is shaded and bounded with a dashed line. Also shown is the cloudy fraction $\langle r^0 \rangle_r \in \{0.7, 0.8, 0.9\}$ indicated by the dotted contours. Fig. 4(b) demonstrates that $r_{\rm eff}$ increases with increasing $N_{\mathcal{D}}$—a trend that implies lower grid-cell averaged reflectivity with increasing S' variability.

Fig. 5 for $\overline{w} = 1$ m/s and $\varepsilon = 0.01$ m^2 s^{-3}, with 5(a) assuming an in-cloud droplet concentration of $N_c = 50$ cm^{-3} while 5(b) assumes 500 cm^{-3}. The figures reveal that $N_{\mathcal{D}}$ spans four orders of magnitude in the range 10^{-2} to 10^2 for a broad range of conditions, and increases with temperature and grid-cell length when σ^2 is assumed constant. In particular, an indirect aerosol effect is observed with $N_{\mathcal{D}}$ increasing linearly with N_c at fixed σ^2. Overall, the estimates of Fig. 5 indicate that the impact of S'-variability on volume-averaged quantities is significant over a wide range of temperatures, droplet concentrations and spatial scales; this result provides strong theoretical support for pursuing stochastic condensation as a subgrid cloud model.

6. Early-time enhanced growth

The analysis of Secs. 5c and 5d exploits the QS approximation which postulates the direct proportionality of $\langle r^3 \rangle_r$ and N_z, independent of $N_{\mathcal{D}}$. Thus a trend toward either evaporation or enhanced growth with increasing $N_{\mathcal{D}}$ is largely prohibited where this assumption is valid. Politovich and Cooper (1988) show that the QS assumption is widely applicable for the case $\mathcal{D}_{\rm FP} = 0$, while Voloshchuk and Sedunov (1977) apply the QS approximation for $\mathcal{D}_{\rm FP} \neq 0$ but do not evaluate its efficacy at large $N_{\mathcal{D}}$. In this section we explore the coupled evolution of $\{G_{\rm FP}, \overline{S}_{\rm FP,G}\}$ for constant $\{\overline{w}, \mathcal{D}_{\rm FP}\}$ without recourse to the QS approximation.

6a. *$\mathcal{B}$ equation*

Returning to Eq. (23), integrating and substituting for $\mathcal{B}$ gives the single ODE

$$\frac{{\rm d}\mathcal{B}}{{\rm d}t} = \frac{c_1 z(t)}{c_0 a^2} - \frac{c_2 a}{c_0}\left\{\frac{\langle r^3\rangle_r}{a^3} - \frac{r_0^3}{a^3}\right\} + \left.\frac{{\rm d}\mathcal{B}}{{\rm d}t}\right|_{t=0} \quad (29)$$

where $c_0 = (2\alpha)^{-1}$ and $\langle r^3 \rangle_r (\mathcal{B}, \mathcal{D}_{\rm FP})$ is again given in Appendix C. In what follows we assume constant $\{\mathcal{D}_{\rm FP}, \overline{w}\}$, $r_0 = 0$, and $d\mathcal{B}/dt|_{t=0} = 0$ corresponding to $\overline{S}_{\rm FP,G}(0) = 0$; the results of this section are therefore conditioned on these initial assumptions.

A comparison of the evolution of $r_{\rm vol} \equiv \langle r^3 \rangle_r^{1/3}$ (left axis) and $\overline{S}_{\rm FP,G}$ (right axis) calculated from Eq. (29) is shown in Fig. 6 for $N_{\mathcal{D}} \in \{0, 5, 10, 15\}$. For $t < 100$ s, a trend toward enhanced growth with increasing $N_{\mathcal{D}}$ is observed in the behavior of $r_{\rm vol}$. This early growth in $r_{\rm vol}$ is described accurately by

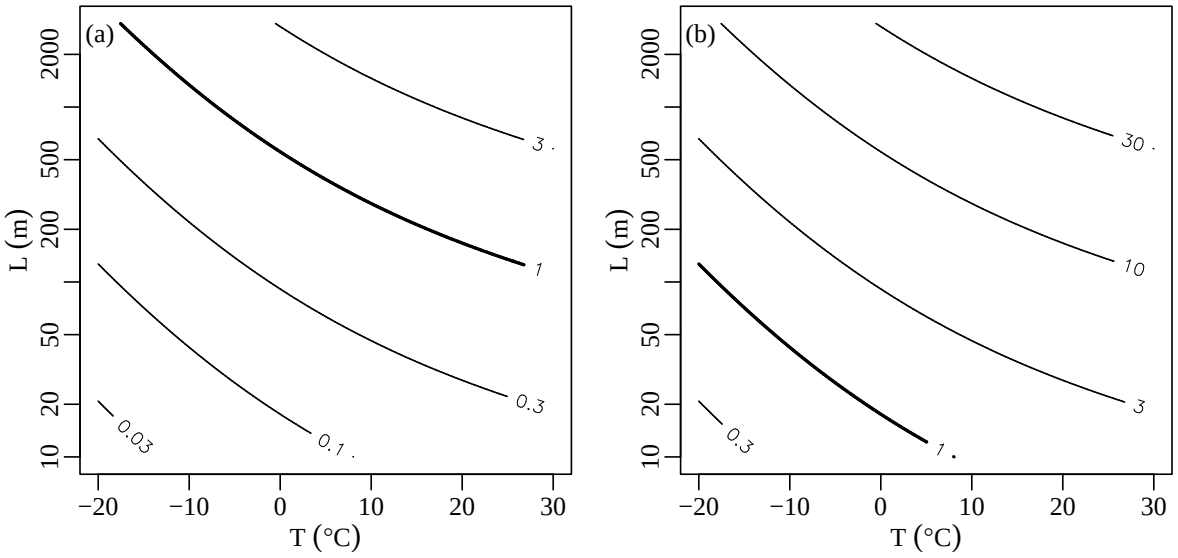

Figure 5: Contour plots of $N_{\mathcal{D}}$ as a function of $\{T, L\}$ for $N_c = 50\ \mathrm{cm}^{-3}$ [Fig. 5(a)] and $N_c = 500\ \mathrm{cm}^{-3}$ [5(b)], typical of clean marine and polluted marine/continental environments, respectively (Heymsfield and McFarquhar 2001). $N_{\mathcal{D}}$ is computed from Eq. (27), assuming $\sigma = 0.01$, $\overline{w} = 1\ \mathrm{m/s}$, the Kolmogorov estimate $\tau = 0.1\varepsilon^{-1/3}L^{2/3}$ and $\varepsilon = 0.01\ \mathrm{m^2\ s^{-3}}$. The figures reveal that a range of $N_{\mathcal{D}}$ values between 10^{-2} and 10^2 exists for typical atmospheric conditions and model grid sizes.

Eq. (20) in the limit $\overline{S} \to 0$ and with the estimate $\langle J \rangle_r = (6a)^{-1}$, obtained as a rough average value from Fig. 3:

$$r_{\mathrm{vol}} \approx \left(\frac{\mathcal{D}_{\mathrm{FP}} t}{8a} \right)^{1/3}$$

valid for $1 \leq r_{\mathrm{vol}} \leq 4\ \mu\mathrm{m}$ where $\langle J \rangle_r$ is approximately constant. This early period of enhanced growth driven by S'-fluctuations and associated with small $\overline{S}$ values has recently been documented by Celani et al. (2005) who performed an (x,z)-2D direct numerical simulation of turbulent velocity and supersaturation fields with 20,000 droplets assuming $\overline{w} = 0$, $c_2 \approx 0$ and $a = 0$. A rapid growth in the in-cloud mean radius, $\overline{r} = \langle r \rangle_r / \langle r^0 \rangle_r$, is shown in their Fig. (6) which is phenomenologically equivalent to the early increase in r_{vol} at large $N_{\mathcal{D}}$ of our Fig. 6[†].

Figure 6 also shows a transition from large positive ($\approx 1\%$) to large negative ($\approx -0.4\%$) $\overline{S}_{\mathrm{FP,G}}$ values as $N_{\mathcal{D}}$ increases with the largest extreme occuring at $t = 20$–30 s. This monotonic decrease in $\overline{S}_{\mathrm{FP,G}}$ with increasing $N_{\mathcal{D}}$ is consistent with the behavior of $\mathcal{B}_{\mathrm{QS}}$ shown in Fig. 4.

The relative impact of the QS approximation on the coupled evolution of $\{f_{\mathrm{FP}}, \mathcal{B}\}$ is further revealed in a graphical comparison of $\mathcal{B}(N_z, N_{\mathcal{D}})$ computed with [Fig. 4(a)] and without [Fig. 7(a)] this assumption. Note that the results of Fig. 7 depend on the relaxation time-scale $\tau_{\mathrm{r}} = a^2 c_0$ (0.025 s) and the number N_w (0.035), in addition to the numbers $\{N_z, N_{\mathcal{D}}\}$. Figure 7(a) exhibits the same qualitative features as 4(a), but there are quantitative differences. Notably, the triple point of the negative $\overline{S}_{\mathrm{FP,G}}$ region has moved to somewhat larger $N_{\mathcal{D}}$ and N_z values: $\{N_{\mathcal{D}} \approx 8.25, N_z \approx 2.0, \mathcal{B} \approx 1.002\}$. In addition the removal of the QS assumption increases the fraction of totally evaporated droplets (dashed lines), and consequently, a greater sensitivity of droplet spectral evolution to the $r = 0$ boundary condition is expected.

Corresponding values of r_{vol}/a are reproduced in Fig. 7(b) where the shaded $\overline{S}_{\mathrm{FP,G}} < 0$ region and dashed lines are again shown. Enhanced growth at early times is clearly apparent with $dr_{\mathrm{vol}}/dN_{\mathcal{D}} > 0$ at fixed N_z, in contrast to the QS assumption which obeys $dr_{\mathrm{vol}}/dN_{\mathcal{D}} = 0$. This behavior implies that the accuracy of the QS assumption **decreases** with increasing $N_{\mathcal{D}}$ in the asymptotic regime $N_z \to 0$

[†]The growth in $\langle r \rangle_r$ predicted by the simulations of Celani et al. is much more gradual than $\overline{r}$, reaching $2.4r_0$ at $t = \tau_L$ (Seminara 2006).

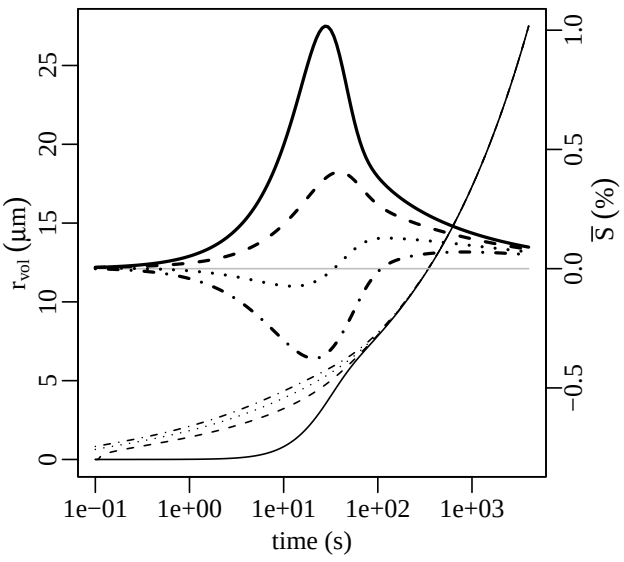

Figure 6: Evolution of $r_{\rm vol}$ (left axis; normal lines) and $\overline{S}_{\rm FP,G}$ (right axis; bold lines) computed from Eq. (29) with $r_0 = 0$, $\tau_{\rm r} = 0.025\,{\rm s}$ and $N_w = 0.035$ for four different $N_{\mathcal{D}}$ values: 0 (—), 5 (- -), 10 ($\cdots$) and 15 ($\cdot - \cdot$). Enhanced growth at early times and decreasing $\overline{S}_{\rm FP,G}$ with increasing $N_{\mathcal{D}}$ is observed. Simulation parameters correspond to $T = 285$ K, $N_c = 100\ {\rm cm}^{-3}$ and $\overline{w} = 1\ {\rm m/s}$.

(and away from the region of negative $\overline{S}_{\rm FP}$), a trend not documented in Voloshchuk and Sedunov (1977). For example, at $N_{\mathcal{D}} = 0$ the QS approximation gives a 3% error in predicted $\mathcal{B}$ at $N_z \approx 80$ (125 s) while the same error in $\mathcal{B}$ at $N_{\mathcal{D}} = 12$ occurs at $N_z \approx 250$ (380 s).

The QS approximation converges to the prediction of Eq. (29) in the limit $t \to \infty$ but it also converges at $d\mathcal{B}/dN_z = 0$ which bounds the shaded region in Fig. 7. Thus the prediction of negative $\overline{S}_{\rm FP}$ has an additional significance:

> For the present initial conditions, prediction of negative $\overline{S}_{\rm FP}$ implies that the QS assumption **underestimates** cloud liquid water while a positive $\overline{S}_{\rm FP}$ implies an **overestimation**.

This conclusion follows from inspection of Eq. (29).

6b. *Spectral broadening*

Although Voloshchuk and Sedunov (1977) provide the first self-consistent derivation of coupled equations for $\{f_{\rm FP}, \overline{S}_{\rm FP}\}$ in terms of a single diffusivity, $\mathcal{D}_{\rm FP}$, they do not analyze the resulting spectra. Subsequent studies, e.g. Manton (1979), Khvorostyanov and Curry (1999a,b), that contain a more detailed spectral analysis neglect the impact of S'-fluctuations on $\overline{S}_{\rm FP}$, and therefore, do not conserve liquid water mass. These studies systematically overestimate $\overline{S}_{\rm FP}$ and, thereby overestimate $\langle r^3 \rangle_r$ and all higher order moments.

Consistent with earlier work (Manton 1979), our closed, adiabatic treatment of $\{f_{\rm FP}, \overline{S}_{\rm FP}\}$ in the absence of droplet coalescence produces a relatively small broadening to larger sizes. This is illustrated in Table 2 which lists the relative impact of $N_{\mathcal{D}}$ on $\langle r^6 \rangle_r$; the moment $\langle r^6 \rangle_r$ is of microphysical relevance because it provides a rough estimate of precipitation efficiency (Berry 1968; Khairoutdinov and Kogan 2000). Consistent with the discussion of Sec. 5f, Table 2 also shows that $\langle r^2 \rangle_r$ decreases with increasing $N_{\mathcal{D}}$ at fixed $r_{\rm vol}$. For the present comparison, $N_{\mathcal{D}} = 0$ is a single-valued spectrum (zero dispersion) and therefore the calculated variation in $\langle r^6 \rangle_r$ and $\langle r^2 \rangle_r$ is an upper bound.

$N_{\mathcal{D}}$ \ $r_{\rm vol}$	$\langle r^2 \rangle_r$ 10	20	50	$\langle r^6 \rangle_r$ 10	20	50
1	0.93	0.96	0.98	1.6	1.3	1.2
3	0.84	0.89	0.94	2.4	1.9	1.5
10	0.71	0.77	0.85	4.5	3.2	2.2
30	0.61	0.65	0.74	8.7	5.8	3.7

Table 2: Table of $\langle r^2 \rangle_r (N_{\mathcal{D}}) / \langle r^2 \rangle_r (0)$ (middle column) and $\langle r^6 \rangle_r (N_{\mathcal{D}}) / \langle r^6 \rangle_r (0)$ (right column) calculated from Eq. (29) at $r_{\rm vol} \in \{10, 20, 50\}$ μm and $N_{\mathcal{D}} \in \{1, 3, 10, 30\}$ with $r_0 = 0$, $\tau_{\rm r} = 0.025\,{\rm s}$ and $N_w = 0.035$. Impact of S'-fluctuations persist to $r_{\rm vol} = 50$ μm; the asymptotic decay $\overline{S}_{\rm FP,G} \sim t^{-1/3}$ of a closed, adiabatic parcel enhances spectral dispersion as compared to earlier estimates (Manton 1979).

In the analysis of Manton (1979, pp. 902), the spectral width of the transition probability $G_{\rm FP}$, Eq. (17), is shown to follow

$$\lim_{t\to\infty} \Delta r \sim \left\{ \frac{\int_0^t {\rm d}\xi\ \mathcal{D}_{\rm FP}(\xi)}{\alpha \int_0^t {\rm d}\xi\ \overline{S}(\xi)} \right\}^{1/2}$$

for $\overline{S} > 0$. Manton further assumes constant $\{\mathcal{D}_{\rm FP}, \overline{S}\}$ which gives constant Δr and dispersion $\Delta r / \langle r \rangle_r \sim t^{-1/2}$. These estimates are inconsistent with the results of Table 2 which indicate broadening

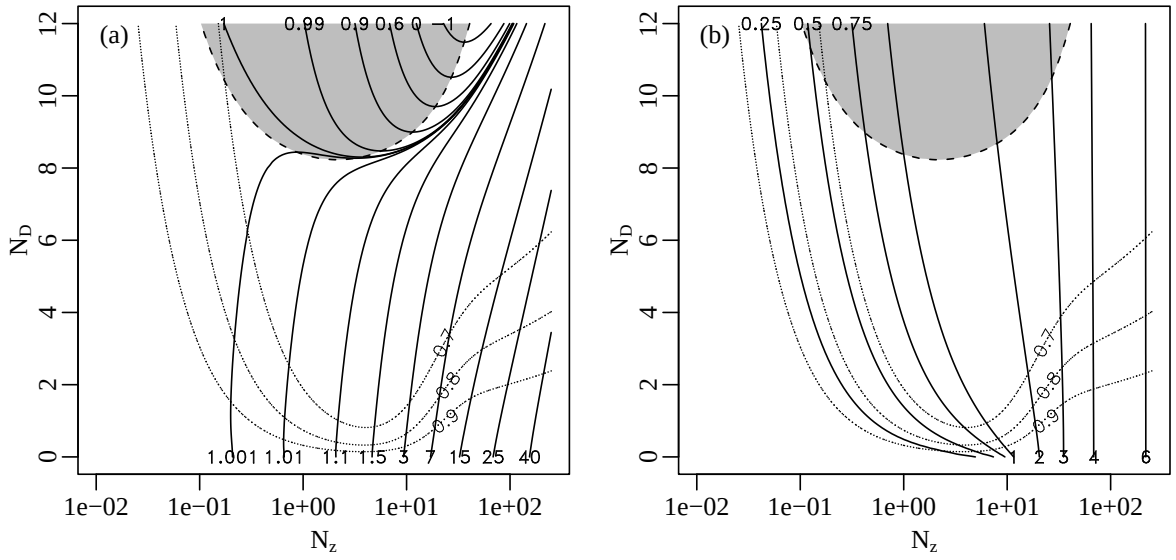

Figure 7: Contour plots of $\mathcal{B}$ [7(a)] and $r_{\rm vol}/a$ [7(b)] as a function of $\{N_z, N_{\mathcal{D}}\}$ calculated from Eq. (29) with $r_0 = 0$, $\tau_{\rm r} = 0.025$ s and $N_w = 0.035$, and indicated by the solid lines. The region where $d\mathcal{B}/dN_z < 0$ and, consequently, $\overline{S}_{\rm FP,G} < 0$ is shaded and bounded with a dashed line. Also shown is the cloudy fraction $\langle r^0 \rangle_r \in \{0.7, 0.8, 0.9\}$ indicated by the dotted contours. A trend toward enhanced growth is revealed in Fig. 7(b) where $dr_{\rm vol}/dN_{\mathcal{D}} > 0$, in contrast to the QS assumption which obeys $dr_{\rm vol}/dN_{\mathcal{D}} = 0$. Simulation parameters correspond to $T = 285$ K, $N_c = 100\ {\rm cm}^{-3}$ and $\overline{w} = 1$ m/s.

that persists to $r_{\rm vol} = 50\ \mu$m. The difference between Manton (1979)'s assumed constant $\overline{S}$ and the asymptotic $\overline{S}_{\rm FP} \sim t^{-1/3}$ of our closed, adiabatic system is the origin of this discrepancy. For the simulations that produced the results of Table 2, Δr broadens slowly with time as $t^{1/6}$ while the dispersion decreases slowly as $t^{-1/6}$.

Table 2 shows that normalized $\langle r^2 \rangle_r$ decreases with decreasing $r_{\rm vol}$, but this trend does not continue as $r_{\rm vol} \to 0$. The minimum value of normalized $\langle r^2 \rangle_r (N_{\mathcal{D}})$ computed from Eq. (29) is shown in Fig. 8 for four values of N_w corresponding to four different droplet concentrations. A few representative values of $r_{\rm vol}(N_{\mathcal{D}})$ are also shown along each of the four lines. Figure 8 reiterates that the impact of S'-fluctuations on droplet spectral evolution becomes significant for $N_{\mathcal{D}}$ values greater than unity and increases monotonically with increasing $N_{\mathcal{D}}$. Minimum values of normalized $\langle r^2 \rangle_r$ occur for $r_{\rm vol}$ in the range 4–14 μm which is of particular significance for cloud shortwave radiative properties. In fact, a survey of effective droplet radius for liquid water clouds using ISCCP satellite observations finds a globally and annually average value of $11.4 \pm 5.6\ \mu$m (Han et al. 1994), which is precisely the size regime where S'-fluctuations have a maximal impact on $\langle r^2 \rangle_r$.

7. Comparison with RICO and SCMS

Underpinning the theory of stochastic condensation is the assumption that the cloud droplet spectrum experiences a complete ensemble of S'-fluctuations. This assumption does not hold for a single cloud parcel with given cloud-base properties that rises stochastically to a given height (Bartlett and Jonas 1972). Recent numerical simulations show that fluctuations in microphysical properties occur below the scale of the parcel, but are small and cause little spectral broadening (Vaillancourt et al. 2001, 2002). Observational studies of droplet spectra and correlations, performed on a cloud-by-cloud basis, reveal evidence of stochastic broadening but are far from definitive. For example, the correlation $\langle \langle r \rangle'_r\, w' \rangle$ from a single horizontal transect through a cumulus cloud shows considerable scatter (Austin et al. 1985), but the mean value is uncertain and this statistic, itself, is disputable because it does not include S'-

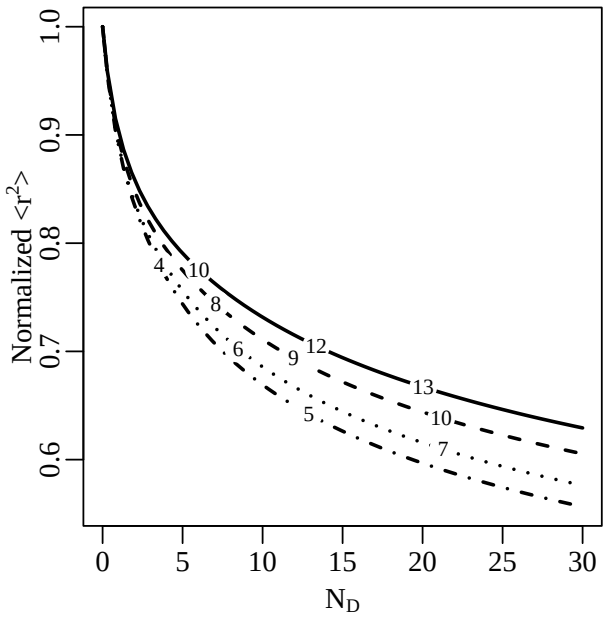

Figure 8: Comparison of the minimum value of $\langle r^2 \rangle_r (N_{\mathcal{D}}) / \langle r^2 \rangle_r (0)$ computed from Eq. (29) with $r_0 = 0$, $\tau_{\rm r} = 0.025$ s and for four different N_w values: 0.07 (—), 0.035 (- -), 0.014 ($\cdots$) and 0.007 ($\cdot - \cdot$), corresponding to $N_c \in \{50, 100, 250, 500\}$ cm^{-3}, respectively, with $T = 285$ K, and $\overline{w} = 1$ m/s. Also shown are representative values of $r_{\rm vol}$ in μm superimposed on each line.

fluctuations associated with temperature/moisture variability and horizontal mixing (Politovich 1993).

Consistent with the present focus on subgrid cloud parameterization, we use a new approach to analyze observed droplet spectra from the Rain In Cumulus over the Ocean (RICO) and Small Cumulus Microphysics Study (SCMS) campaigns that is a significant departure from the traditional "parcel" analysis. In particular, we consider droplet spectra averaged over segments of length, L, which may contain several clouds of varying size and liquid water density. This spectral averaging is constrained by the segment-averaged liquid-water density, $\langle \rho_l \rangle$, which must lie in a given narrow range. Our underlying assumption is that the spectra averaged in this fashion approximate the true grid-averaged droplet spectra that a cloud parameterization "should" provide, for a given grid size L and grid-averaged $\langle \rho_l \rangle$.

A seminal feature of the present analysis is the prediction that $\mathcal{D}_{\rm FP}$, and hence $N_{\mathcal{D}}$, increases with scale, L, as demonstrated in Fig. 5. We find evidence of spectral broadening in the RICO/SCMS spectra that increases with L, and we use the spectra themselves, and not a correlation such as $\langle \langle r \rangle_r' \, w' \rangle$, to infer the L-dependence and size of $N_{\mathcal{D}}$.

7a. *Observational datasets*

i. RICO/SCMS Both the RICO and SCMS campaigns targeted fields of cumulus clouds with RICO focusing on shallow, maritime, trade wind cumulus while SCMS targeted shallow cumulus clouds in Florida. Both projects included the statistical sampling of cumulus cloud fields using a series of constant altitude flight legs that attempt to gather a complete ensemble of cloud properties. Thus these data sets are well suited to the study of stochastic condensation. Our RICO analysis utilizes observations from 11 flights of the NCAR C-130 that targeted the statistical sampling of non-precipitating trade wind cumulus: RF-$\{$1,3,4,6,7,9,10,12,13,14,18$\}$ (JOSS 2005). For SCMS we use the same four NCAR C-130 flights analyzed and validated by Rodts et al. (2003) as a baseline: RF-$\{$12,13,16,17$\}$. The cloud statistics and spectra that we report are obtained from the NCAR FSSP-100 probe. This data set, measured at 10 hz and post-processed according to RAF (2006b,a), is smoothed once using a nearest-neighbor filter with weights $\{$1/4,1/2,1/4$\}$; otherwise no further post-processing is performed. The analysis of this section rests on the assumption that the RICO/SCMS flight segments represent a complete, unbiased ensemble of cumulus cloud statistics. See Rodts et al. (2003) for a detailed discussion of this assumption.

ii. Statistics The distribution of cloud sizes from RICO and SCMS is compared in Fig. 9(a) for cloud lengths between 100 and 7500 meters. Previous studies have shown that cumulus cloud sizes obey a power law distribution for sizes smaller than an outer length. This is verified in Fig. 9(a) which shows an increase in the decay of the size distribution beginning near ≈ 1000 m, consistent with previous results (Rodts et al. 2003).

We proceed to calculate cloud and droplet statistics averaged over segments of length $L_1 \leq L \leq L_2$ and over liquid water densities in the range, $\rho_1 \leq \langle \rho_l \rangle \leq \rho_2$. Statistics are calculated for six length bands: $L_1 \in 100, 200, 500, 1000, 2000, 5000$ and $L_2 \in 150, 300, 750, 1500, 3000, 7500$, respectively. For the RICO dataset four density bands (in g/m^3) are selected: $\rho_1 \in \{0.01, 0.02, 0.05, 0.1\}$ and $\rho_2 \in \{0.02, 0.05, 0.1, 0.5\}$, respectively, while two density bands are chosen for SCMS: $\rho_1 \in \{0.02, 0.05\}$ and

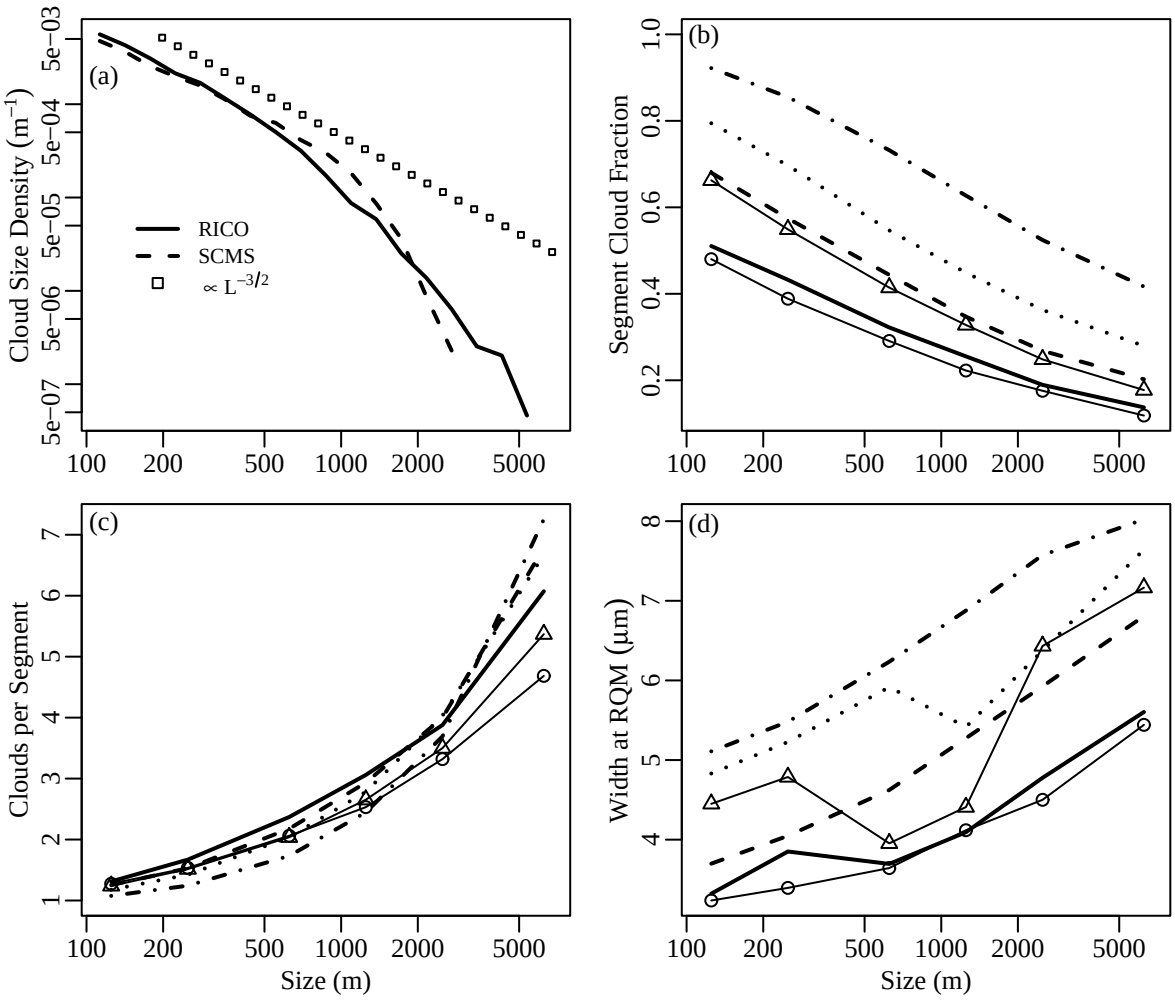

Figure 9: Cloud and droplet-spectrum statistics computed from the RICO and SCMS datasets described in the text using a cloud threshold of 7 cm^{-3} (Rodts et al. 2003). Fig 9(a) shows the distribution of cloud sizes between 100 and 7500 meters; a scale-break near 1000 m is evident (Rodts et al. 2003). For Figs. 9(b) through (d) the abscissa represents the length of an observational segment that may contain several clouds. Segment statistics are binned according to segment-averaged liquid-water density $\langle \rho_l \rangle$ (in $\mathrm{g/m}^3$) for RICO (bold lines): 0.01–0.02 (—), 0.02–0.05 (- -), 0.05–0.01 ($\cdots$), 0.1–0.5 ($\cdot - \cdot$), and for SCMS (lines+symbols): 0.02–0.05 (◯), 0.05–0.2 (△). Cloud fraction, which decreases with increasing L, is shown in Fig. 9(b), while Fig. 9(c) shows cloud number which increases with increasing L. A comparison of spectral width at Right-Quarter-Maximum (RQM), computed from the segment-averaged droplet spectrum recorded by the FSSP-100, is given in Fig. 9(d). Spectral dispersion increases with increasing L, consistent with theoretical considerations of stochastic condensation from Sec. 5g.

$\rho_2 \in \{0.05, 0.2\}$, respectively. A total of about 3.5 million distinct segments are included in the RICO analysis while around half-a-million segments make up the SCMS dataset. Segment in-cloud number concentration, N_c, increases with increasing $\langle \rho_l \rangle$; a straightforward average of the average value for each of the six length bands (in cm^{-3}) gives $N_c \in \{42 \pm 11, 53 \pm 10, 65 \pm 8, 88 \pm 6\}$, respectively, for RICO and $N_c \in \{113 \pm 31, 146 \pm 22\}$, respectively, for SCMS. Increasing $\langle \rho_l \rangle$ is also associated with decreasing temperatures, $\langle T \rangle$. The same averaging procedure for temperature (i.e. an average of the six average values) gives (in C°) $\langle T \rangle \in \{18.7 \pm 0.1, 18.0 \pm 0.2, 17.2 \pm 0.6, 15.7 \pm 0.8\}$, respectively, for RICO and $\langle T \rangle \in \{19.3 \pm 0.2, 18.5 \pm 0.4\}$ for SCMS.

A plot of segment cloud fraction as a function of L is shown in Fig. 9(b). Segment cloud fraction decreases monotonically with increasing L as expected. It also increases monotonically with increasing $\langle \rho_l \rangle$ which reflects the fact that increasing cloud area, and not just increasing **in-cloud** liquid water density (see N_c above), is contributing to increase segment $\langle \rho_l \rangle$. As segment cloud fraction decreases with increasing L, we expect the number of clouds per segment to increase, and this is verified in Fig. 9(c). Unlike segment cloud fraction, no clear trend in cloud number with increasing $\langle \rho_l \rangle$ is evident. Figures 9(b) and (c) demonstrate good correspondence in the cumulus cloud statistics generated from the RICO and SCMS datasets. Overall, the SCMS segments contain somewhat fewer clouds and a significantly smaller cloud fraction than the RICO segments at a given $\langle \rho_l \rangle$.

The present model of stochastic condensation predicts increasing droplet spectral dispersion with increasing L. However, great care must be taken in the selection of an approximate statistic to measure this broadening in observational data. For our purposes, an appropriate measure of stochastic broadening must be insensitive to both the largest drops (which are affected by collision-coalescence) and the smallest (which are poorly measured by the FSSP-100). The width of the droplet radius spectrum from mode to Right-Quarter-Maximum (RQM)[†] satisfies both of these criteria and is shown in Fig. 9(d) as a function of segment length L. For density bands 2 through 4 of the RICO spectra, the location of the spectral maximum and RQM fall between 3.9 $\mu\mathrm{m}$ (bin 6) and 15 $\mu\mathrm{m}$ which excludes both the lower size range where the FSSP-100 is inaccurate (bins 3-4) and the larger sizes where collision-coalescence dominates. Extraction of the spectral maximum for RICO density band 1 depends on bin 5 (3.1 $\mu\mathrm{m}$) which may be less accurate. For SCMS, the width-at-RQM is less accurately measured because the spectral resolution is coarser (15 vs 28 total bins for RICO) and the spectral maximum are at smaller sizes as a result of larger droplet number concentrations.

Overall, Fig. 9(d) demonstrates increasing spectral dispersion (as measured by the width-at-RQM) with increasing L as expected from the theory of stochastic condensation. Increasing width-at-RQM with increasing $\langle \rho_l \rangle$ is also exhibited. While these trends may appear obvious upon first consideration, the straightforward averaging of spectra is, in contrast, L-independent by definition—summation is invariant under re-ordering and re-grouping. It is only the constraint of fixed $\langle \rho_l \rangle$ that allows the L-dependence to emerge. It is encouraging that the overall trend in width-at-RQM vs L is consistent across the RICO and SCMS datasets and density bands; this is suggestive of a common underlying physics that may be captured in a single subgrid modeling framework.

7b. *Spectral broadening and* $N_{\mathcal{D}}$

Atmospheric models are typically required to predict the evolution of the grid-cell averaged droplet spectrum, $f(r)$, or at least several of its moments, given a set of prognosed quantities at the grid-scale including $\langle \rho_l \rangle$. As shown in Figs. 9(b) and (c), a model grid-cell of (horizontal) size ≥ 100 meters containing cumulus will have a cloud fraction less than unity and may contain several clouds. Thus the grid-cell averaged spectrum will, in general, be distinct from the spectrum observed in, or averaged over, a single given cloud.

The six RICO spectra for density band 3, $0.05 \leq \langle \rho_l \rangle \leq 0.1$ in $\mathrm{g/m}^3$, are shown in Fig. 10(a) with unit normalization. The average single-measurement ($L =$ FSSP resolution) spectrum for the same $\langle \rho_l \rangle$ range is also reproduced (dotted line). Note that the local spectral maximum at 1.5 $\mu\mathrm{m}$ is in the small size regime where the FSSP-100 data quality is poor and is, subsequently, ignored. These spectra indicate that, for cumulus clouds, the shape of $f(r)$ is strongly L-dependent. This behavior is in contradistinction to the common modeling assumption that $f(r)$ obeys a log-normal or gamma distribution that is independent of L. In addition to the increase in width-at-RQM with increasing L documented in Fig. 9(d), Fig. 10(a) indicates a decrease in skewness with increasing L.

The observational spectra shown in Fig. 10(a)

[†]The radius larger than (i.e. to the right of) the mode where f drops to 1/4 of its maximum.

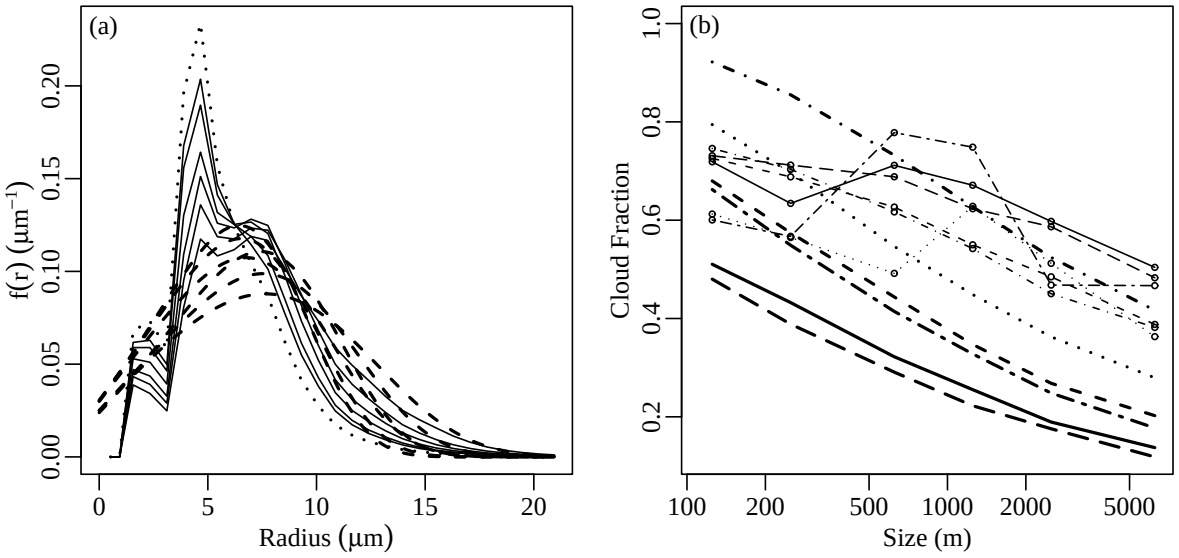

Figure 10: Comparison of observed droplet spectra [Fig. 10(a)] and cloud fraction [10(b)] vs model predictions. The observed spectra in 10(a) are computed for density band 3, $0.05 \leq \langle \rho_l \rangle \leq 0.1$ g/m^3: six spectra (—), corresponding to six L values (see text), and the single-point spectrum ($\cdots$) are shown, with the spectral peak decreasing monotonically with increasing L. Parameter values for the corresponding modeled spectra (- -), computed from Eq. (28), are retrieved by matching width-at-RQM and $\overline{r}$ to the observed values. Fig. 10(b) shows cloud fraction vs L for all observed (bold lines) and modeled (lines+symbols) density bands (in g/m^3) for RICO: 0.01–0.02 (—), 0.02–0.05 (- -), 0.05–0.01 ($\cdots$), 0.1–0.5 ($\cdot - \cdot$), and for SCMS: 0.02–0.05 ($- -$), 0.05–0.2 ($\cdot$ — $\cdot$). The observed spectra and cloud fraction statistics show evidence of non-Gaussian S' statistics and inhomogeneous mixing, in contradistinction to the assumptions of the present Fokker-Planck approach.

can be used to retrieve $\{N_z, N_{\mathcal{D}}\}$ using the present model of stochastic condensation in the QS limit, Eq. (28). We perform this retrieval by matching two statistics of the model to the data: (i) width-at-RQM and (ii) in-cloud mean radius, $\overline{r} = \langle r \rangle_r / \langle r^0 \rangle_r$. The six retrieved spectra, corresponding to the six observational spectra for density band 3, are also shown in Fig. 10. Qualitatively, the two sets of spectra are similar with pronounced broadening in the "core" region between 3 and 15 μm that increases with increasing L. However, important differences are also evident. In particular, the observational spectra exhibit a sharp spectral peak between 3.5 and 6 μm that is not produced by the present model. In related fashion, the modeled spectra predict a significant fraction of droplets in the 0–3 μm regime that is not supported by the observations.

We attribute the cause of these differences to a key underlying assumption of the present theory of stochastic condensation which can be phrased in two equivalent ways: (i) S', itself, is assumed normally distributed, as per Sec. 2, or (ii) the assumed Fokker-Planck renormalization $\tau \to 0$ gives a normal distribution of $\int_0^t \mathrm{d}\xi \; S'(\xi)$, independent of the S'-distribution. The equivalent result of either assumption is that a sizable portion of droplets experience a vanishingly small, but non-zero, negative supersaturation that permits them to exist in the 0–3 μm regime for extended periods before evaporating completely. This phenomenological picture is distinct from Baker et al. (1980)'s model of extreme inhomogeneous mixing in which a fraction of droplets evaporate completely during a mixing event while the remainder are unchanged. Thus Baker et al.'s model corresponds to a distribution of S' values that is strongly peaked near zero and near the negative supersaturation of unmixed environmental air. Support for this highly non-Gaussian distribution of S' values is found in a new PDF model of cloud mixing and evaporation (Jeffery and Reisner 2006).

Further support for non-Gaussian S' statistics and inhomogeneous mixing is found in Fig. 10(b) which

shows a comparison of the observed cloud fractions, CF, (reproduced from Fig. 9(b)) and modeled cloud fractions, $\langle r^0 \rangle_r$. Strictly speaking, $\langle r^0 \rangle_r$ is not equivalent to observational CF; $f(r)$ does not provide spatial information and some volume fraction of the "labels" (e.g. CCN) of completely evaporated droplets may reside within cloudy air. Yet, overall, at large L the observational spectra exhibit, simultaneously, small cloud fractions (five out of six density bands with $0.1 < \mathrm{CF} < 0.3$) and well-defined spectral peaks, while the modeled spectra have larger cloud fractions ($0.35 < \langle r^0 \rangle_r \leq 0.5$) and significant broadening to smaller sizes. Thus Fig. 10(b) reiterates the importance of accounting for the inhomogeneous mixing processes—allowing for the complete evaporation of droplets **without** significant broadening to smaller sizes—in the formulation of stochastic models of grid-averaged spectra.

Lastly, the values of $N_{\mathcal{D}}$ retrieved from the observational RICO/SCMS spectra are shown in Fig. 11. Also shown in the figure is a shaded region calculated using the theoretical estimate from Sec. 5g which assumes $\tau \sim L^{2/3}$ and a constant, L-independent S'-variance. Observed values of $\langle T \rangle$ and N_c are used to estimate $N_{\mathcal{D}}$; the shaded region is defined by an upper bound calculated from the SCMS data (larger $\langle T \rangle$ and N_c) and a lower bound from RICO (smaller $\langle T \rangle$ and N_c). The pattern of retrieved $N_{\mathcal{D}}$ values shares similarities with the retrieved widths at RQM (Fig. 9(d)), although $N_{\mathcal{D}}$ does not exhibit a similar dependence on $\langle \rho_l \rangle$. For large scales, $L \geq 500$ m, the retrieved $N_{\mathcal{D}}$ values are broadly consistent with the estimates of Fig. 5 despite the very crude (order of magnitude) estimate of $\mathcal{D}_{\mathrm{FP}}$. For smaller scales, $L < 500$ m, the retrieved values of $N_{\mathcal{D}}$ appear to be overestimated. We attribute this overestimation to the lack of aerosol physics (sub-cloud distributions, activation, recycling) and collision-coalescence in the present approach which leads to a dispersion-less spectrum as $L \to 0$.

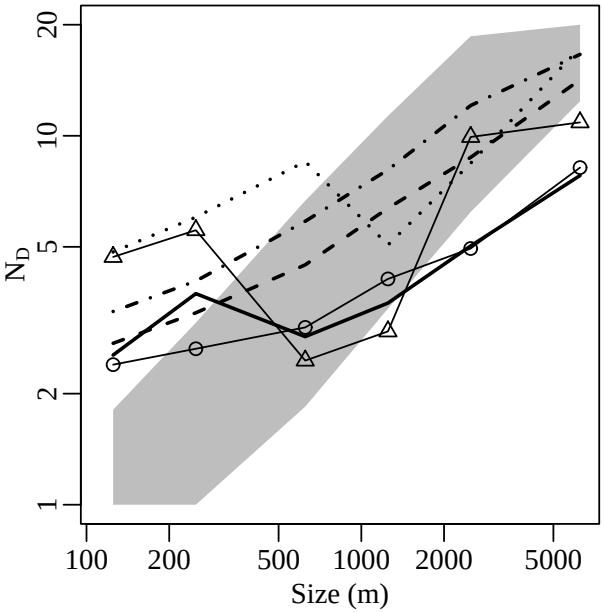

Figure 11: Retrieved values of $N_{\mathcal{D}}$ for all six segment lengths and all RICO (4) and SCMS (2) density bands. Line types for the six density bands as per Fig. 9(b)–(d); see Fig. 9 caption for further details. Also shown are the theoretical estimates of $N_{\mathcal{D}}$ (shaded region) from Sec. 5g using observed values of $\{\langle T \rangle, N_c\}$ from SCMS (region upper bound) and RICO (region lower bound). The theoretical estimates assume $N_{\mathcal{D}} \sim L^{2/3}$ which agrees well with retrieved $N_{\mathcal{D}}$ values at large L.

8. Summary

In this work we have taken "another look" at stochastic condensation in the hope of clarifying the earlier derivations and fully exploring the implications of this approach for subgrid cloud parameterization. In contrast to the derivations of Levin and Sedunov (1966a,b, 1967) and Manton (1979), we begin with a simple model of stochastic condensation—independent, Gaussian supersaturation fluctuations (S') renewed after a time τ—that is exactly solvable. This model is appropriate for subgrid cloud modeling where $t \gg \tau$ is not generally satisfied and can be used to compare and contrast Lagrangian and Eulerian approaches for modeling droplet spectra (Andrejczuk et al. 2006). The Fokker-Planck approximation to this exact solution follows by replacing the discrete sampling of S' with its continuous surrogate. The Fokker-Planck diffusivity, $\mathcal{D}_{\mathrm{FP}}$, is thus seen to be the natural smooth-in-time approximation to a discrete-in-time process. The contributions of $\mathcal{D}_{\mathrm{FP}}$ to the evolution equation for the r-moments are given in Eq. (20); these new subgrid terms are easily incorporated into moment-based cloud schemes that resolve supersaturation.

We have also taken another look at the equation for the mean supersaturation, $\overline{S}_{\mathrm{FP}}$, in the presence of S' fluctuations modeled using Fokker-Planck theory. While this problem is treated in an approximate fashion (and with little transparency) in

Voloshchuk and Sedunov (1977), we derive the expression for $\langle S'|r\rangle_{\rm FP}$ without approximation and show how this expression "closes" the $\overline{S}_{\rm FP}$-equation self-consistently, thereby ensuring that total water mass is exactly conserved. Using the quasi-stationary (QS) evaluation of $\overline{S}_{\rm FP}$, we derive the exact correction term to $\overline{S}_{\rm FP,QS}$ (i.e. the S' contribution corresponding to the Fokker-Planck model). The correction term is negative definite, peaks in magnitude when $\langle r\rangle_r$ is near the accommodation length ($\approx 2\ \mu$m), and decays as $\langle r^{-1}\rangle_r$ as the droplet spectrum grows to large sizes. This exact result has a direct correspondence to the analysis of Cooper (1989). Using our self-consistent equation for $\overline{S}_{\rm FP}$, we evaluate spectral broadening in an adiabatic volume (grid-cell or grid-column) and find some broadening to larger sizes (consistent with earlier estimates, e.g. Manton (1979)), but a more significant decrease in $\langle r^2\rangle_r$ at fixed liquid water content which may have implications for modeled cloud reflectivity.

While the proceeding discussion is largely a clarification and elucidation of previous work, most notably Voloshchuk and Sedunov (1977), we have also extended the theory of stochastic condensation by deriving the non-dimensional number, $N_{\mathcal{D}}$, that determines the relative impact of S'-fluctuations on droplet spectral evolution in an adiabatic volume and in the QS limit. For constant updraft velocity and $\mathcal{D}_{\rm FP}$, $N_{\mathcal{D}}$ is also a constant, ranging from 10^{-2} to 10^2 for typical atmospheric conditions and model grid sizes when the assumed S'-standard deviation is 1%. We find significant spectral broadening, and in particular decreasing $\langle r^2\rangle_r$, for $N_{\mathcal{D}} > 1$, and discover that $\overline{S}_{\rm FP,QS}$ can be negative in a partially cloudy grid-cell when $N_{\mathcal{D}} > 6.5$ for droplets of zero initial size. The information provided by $N_{\mathcal{D}}$ is of direct relevance to the implementation of stochastic condensation in a subgrid cloud scheme where both (i) a priori estimates of $\mathcal{D}_{\rm FP}$ and (ii) a posteriori diagnostics of the relative importance of $\mathcal{D}_{\rm FP}$, are needed.

Using in-situ droplet spectra from cumulus cloud fields observed during the RICO and SCMS field campaigns, we have verified a seminal prediction of the theory of stochastic condensation—increasing broadening with increasing spatial scale—by averaging the observed spectra over segments containing one or more clouds. In addition, scale-dependent values of $N_{\mathcal{D}}$ retrieved from the segment-averaged spectra using our adiabatic model show good consistency with the previously discussed theoretical estimates. While past studies of stochastic condensation emphasize the spectral broadening observed in spectra from individual clouds, we believe that our scale-dependent analysis of observed spectra is the correct approach for understanding and assessing the efficacy of stochastic condensation as a subgrid cloud model. Moreover, our results suggest that the parameterization of unresolved S'-fluctuations using Fokker-Planck theory or other means will become increasingly important as explicit (bin) microphysics schemes are applied at larger scales (Lynn et al. 2005), where an increasing fraction of individual clouds are, themselves, unresolved.

However, important differences between the observed and modeled droplet spectra are also observed. In particular, the observed spectra suggest non-Gaussian S' fluctuations and the inhomogeneous mixing process of Baker et al. (1980). Further work is needed to assess the impact of non-Gaussian S'-fluctuations and large renewal times on droplet spectral broadening and to derive differential operators that can model their ensemble effect in the equations of cloud physics. This line of investigation is currently being pursued.

Acknowledgement This work was funded by a Los Alamos National Laboratory Directed Research and Development Project entitled "Resolving the Aerosol-Climate-Water Puzzle (20050014DR)". We thank Nicole Jeffery for her comments on this manuscript. The lead author is indebted to the "Crisis Points" program (1996-2000) of the Peter Wall Institute for Advanced Studies which provided the foundation for this work.

A. Thermodynamic constants

The constant α defined in Eq. (4) is (Pruppacher and Klett 1997, Eq. (13-28))

$$\alpha = (\rho_s/\rho_w) D_v G$$

where

$$G = \left\{ 1 + \frac{\rho_s}{\rho_d} \frac{L_v}{c_p T} \left(\frac{L_v}{R_v T} - 1 \right) \right\}^{-1},$$

ρ_s is saturation vapor density, ρ_d is air density, ρ_w is water density, D_v is molecular diffusivity of vapor, L_v is latent heat of vaporization, c_p is heat capacity, R_v is water vapor gas constant, T is temperature, and we have assumed equality of the conductivities of vapor and temperature.

The constant c_1 of Eq. (21) is (Pruppacher and Klett 1997, Eq. (13-29))

$$c_1 = \frac{L_v}{R_v T^2} \frac{g}{c_p} - \frac{g}{R_d T}$$

where g is gravitational acceleration and R_d is the gas constant of air. To good approximation the constant c_2 is

$$c_2 = (4/3)\pi D_v N_c/\alpha$$

where N_c is droplet concentration.

B. Derivation of N_w, $N_{\mathcal{D}}$ and $N_{\mathcal{D},\overline{S}}$

The non-dimensional number N_w along with N_z determines $\overline{S}_{\rm QS}$ in the case $\sigma^2 = 0$. Let

$$N_w(t) \equiv \frac{c_1}{c_2 a \alpha}\overline{w}(t).$$

Then solving Eq. (22) for $\overline{S}_{\rm QS}$ gives

$$\overline{S}_{\rm QS} = \frac{N_w}{3}\left(\frac{r_0^3}{a^3}+N_z\right)^{-2/3}\left\{1+\left(\frac{r_0^3}{a^3}+N_z\right)^{1/3}\right\}$$

which illustrates how the two numbers $\{N_z, N_w\}$ combine to modulate $\overline{S}$. For the special case of constant $\overline{w}$ we have the asymptotic

$$\lim_{N_z\to\infty}\overline{S}_{\rm QS} \sim N_z^{-1/3} \sim t^{-1/3}$$

which shows that $\overline{S}_{\rm QS}$ decays as the parcel rises. For the regime $r_0^3/a^3 \ll N_z \ll 1$ we have

$$\overline{S}_{\rm QS} \sim N_z^{-2/3} \sim t^{-2/3}$$

which exhibits a faster decay.

The non-dimensional number $N_{\mathcal{D}}$ determines the relative impact of S'-fluctuations on the r-moments. It cannot be derived on the basis of dimensional analysis alone since the parameter $a^{-4}\int_0^t {\rm d}\xi\ \mathcal{D}_{\rm FP}(\xi)$ is a non-dimensional group. Instead, we consider the case $f_{\rm FP} = G_{\rm FP}$ and expand the analytic expression for $\left\langle r^3\right\rangle_r$ (see appendix C) to first order in small parameter $\int_0^t {\rm d}\xi\ \mathcal{D}_{\rm FP}(\xi)/\beta^2$ where $\beta = (r_0+a)^2 + 2\alpha\int_0^t {\rm d}\xi\ \overline{S}_{\rm FP,G}(\xi)$:

$$\begin{aligned}\left\langle r^3\right\rangle_r &= \beta^{3/2}\left\{1+\frac{3\int_0^t {\rm d}\xi\ \mathcal{D}_{\rm FP}(\xi)}{4\beta^2}\right\} - 3a\beta \\ &\quad +3a^2\beta^{1/2}\left\{1-\frac{\int_0^t {\rm d}\xi\ \mathcal{D}_{\rm FP}(\xi)}{4\beta^2}\right\} - a^3\end{aligned}$$

Substituting this result into Eq. (28) and rearranging gives

$$\left(\mathcal{B}_{\rm QS}^{1/2}-1\right)^3 = \frac{r_0^3}{a^3}+N_z\left\{1-\frac{3}{4}\frac{N_{\mathcal{D}}}{\mathcal{B}_{\rm QS}^{1/2}}+\frac{3}{4}\frac{N_{\mathcal{D}}}{\mathcal{B}_{\rm QS}^{3/2}}\right\} \quad (30)$$

where $N_{\mathcal{D}}$ is defined by Eq. (27).

If either $\overline{w}$ or $\mathcal{D}_{\rm FP}$ is time-dependent then the number

$$N_{\mathcal{D},\overline{S}} \equiv \frac{c_2 a}{c_1\alpha}\frac{\mathcal{D}_{\rm FP}(t)}{z(t)},$$

along with N_w, determines the relationship between $\overline{S}$ and $\{\mathcal{B}_{\rm QS}, N_z, N_{\mathcal{D}}\}$.

C. $G_{\rm FP}$ moments

Equations (28) and (29) require the evaluation of $\left\langle r^3\right\rangle_r$. For $G_{\rm FP}$ defined by Eq. (17) an analytic expression for $\left\langle r^3\right\rangle_r$ is available if the lower bound, $r = 0$, on the integration over $G_{\rm FP}$ is replace by $r = -a$. We have verified that this approximation is valid for $\left\langle r^3\right\rangle_r$ where the dominant contribution comes from $r \gg 0$.

Defining $\gamma = \int_0^t {\rm d}\xi\ \mathcal{D}_{\rm FP}(\xi)$ and $\lambda = \beta^2/(4\gamma)$ with $\beta = (r_0+a)^2 + 2\alpha\int_0^t {\rm d}\xi\ \overline{S}_{\rm FP}(\xi)$, the moments of $G_{\rm FP}$ with support $[-a,\infty]$ are

$$\begin{aligned}\left\langle (r+a)^0\right\rangle_r &= {\rm erfc}\left(-\sqrt{\lambda}\right)/2 \\ \left\langle (r+a)^1\right\rangle_r &= \frac{e^{-\lambda}}{\sqrt{2\pi}\gamma^{1/4}}\{\sqrt{\gamma}\Gamma(3/4)F_{1,1}(3/4,1/2,\lambda) \\ &\quad +\beta\Gamma(5/4)F_{1,1}(5/4,3/2,\lambda)\} \\ \left\langle (r+a)^2\right\rangle_r &= \frac{\beta}{2}{\rm erfc}\left(-\sqrt{\lambda}\right)+\left(\frac{\gamma}{\pi}\right)^{1/2}e^{-\lambda} \\ \left\langle (r+a)^3\right\rangle_r &= \frac{\gamma^{1/4}e^{-\lambda}}{2\sqrt{2\pi}}\{\sqrt{\gamma}\Gamma(1/4)F_{1,1}(5/4,1/2,\lambda) \\ &\quad +3\beta\Gamma(3/4)F_{1,1}(7/4,3/2,\lambda)\} \\ \left\langle (r+a)^4\right\rangle_r &= \frac{1}{2}(2\gamma+\beta^2){\rm erfc}\left(-\sqrt{\lambda}\right)+\left(\frac{\gamma}{\pi}\right)^{1/2}\beta e^{-\lambda} \\ \left\langle (r+a)^5\right\rangle_r &= \frac{3\gamma^{3/4}e^{-\lambda}}{16\sqrt{2\pi}}\{16\sqrt{\gamma}\Gamma(3/4)F_{1,1}(7/4,1/2,\lambda) \\ &\quad -5\beta\Gamma(-3/4)F_{1,1}(9/4,3/2,\lambda)\} \\ \left\langle (r+a)^6\right\rangle_r &= \frac{\beta}{2}(6\gamma+\beta^2){\rm erfc}\left(-\sqrt{\lambda}\right)+\left(\frac{\gamma}{\pi}\right)^{1/2}(4\gamma+\beta^2)e^{-\lambda}\end{aligned}$$

These expressions are used to calculate $\langle r^n\rangle_r$ with $n \in \{2,3,6\}$. In particular

$$\left\langle r^3\right\rangle_r = \left\langle (r+a)^3\right\rangle_r - 3a\left\langle (r+a)^2\right\rangle_r + 3a^2\left\langle (r+a)^1\right\rangle_r - a^3\left\langle (r+a)^0\right\rangle_r \quad (31)$$

References

Andrejczuk, M., J. M. Reisner, and C. A. Jeffery, 2006: Comparison of analytical solutions for the growth of cloud droplets against Eulerian and Lagrangian numerical formulations. *Mon. Wea. Rev.*, to be Submitted.

Austin, P. H., M. B. Baker, A. M. Blyth, and J. B. Jensen, 1985: Small-scale variability in warm continental cumulus clouds. *J. Atmos. Sci.*, **42**, 1123–1138.

Baker, M. B., R. G. Corbin, and J. Latham, 1980: The influence of entrainment on the evolution of cloud droplet spectra: I. A model of inhomogeneous mixing. *Quart. J. Roy. Meteor. Soc.*, **106**, 581–599.

Bartlett, J. T. and P. R. Jonas, 1972: On the dispersion of the sizes of droplets growing by condensation in turbulent clouds. *Quart. J. R. Met. Soc.*, **98**, 150–164.

Belyaev, V. I., 1961: The size distribution of drops in a cloud in the condensation stage of development. *Bull. (Izv.) Acad. Sci. USSR, Geophys. Ser.*, **8**.

Berry, E. X., 1968: Modification of the warm rain process. *Proc. First Natl. Conf. Weather modification*, Am. Meteorol. Soc., Albany, NY, 81–88.

Celani, A., G. Falkovich, A. Mazzino, and A. Seminara, 2005: Droplet condensation in turbulent flows. *Europhys. Lett.*, **70**, 775–781.

Cooper, W. A., 1989: Effects of variable droplet growth histories on droplet size distributions. Part I: Theory. *J. Atmos. Sci.*, **46**, 1301–1311.

Han, Q., W. B. Rossow, and A. A. Lacis, 1994: Near-global survey of effective droplet radii in liquid water clouds using ISCCP data. *J. Climate*, **7**, 465–497.

Heymsfield, A. J. and G. M. McFarquhar, 2001: Microphysics of INDOEX clean and polluted trade cumulus clouds. *J. Geophys. Res.*, **106**, 28653–28673.

Jeffery, C. A. and J. M. Reisner, 2006: A study of cloud mixing and evolution using PDF methods. 1. Cloud front propagation and evaporation. *J. Atmos. Sci.*, in press.

JOSS, 2005: RICO mission table, `http://www.joss.ucar.edu/rico/catalog/missions`.

Khairoutdinov, M. and Y. Kogan, 2000: A new cloud physics parameterization in a large-eddy simulation model of marine stratocumulus. *Mon. Wea. Rev.*, **128**, 229–243.

Khvorostyanov, V. I. and J. A. Curry, 1999a: Toward the theory of stochastic condensation in clouds. Part I: A general kinetic equation. *J. Atmos. Sci.*, **56**, 3985–3996.

— 1999b: Toward the theory of stochastic condensation in clouds. Part II: Analytical solutions of the gamma-distribution type. *J. Atmos. Sci.*, **56**, 3997–4013.

Levin, L. M. and Y. S. Sedunov, 1966a: A kinetic equation describing microphysical processes in clouds. *Doklady Akad. Nauk SSSR*, **170**, 4–6.

— 1966b: Stochastic condensation of drops and kinetics of cloud spectrum formation. *J. Rech. Atmos.*, **2**, 425–432.

— 1967: Kinetics of the formation of a cloud spectrum. *Atmos. Ocean. Phys.*, **3**, 242–248.

Lynn, B. H., A. P. Khain, J. Dudhia, D. Rosenfeld, A. Pokrovsky, and A. Seifert, 2005: Spectral (bin) microphysics coupled with a mesoscale model (MM5). Part I. Model description and first results. *Mon. Wea. Rev.*, **133**, 44–58.

Manton, M. J., 1979: On the broadening of a droplet distribution by turbulence near cloud base. *Quart. J. R. Met. Soc.*, **105**, 899–914.

Mazin, I. P., 1965: Theory of formation of a particle-size spectrum in clouds and precipitation. *Trans. (Trudy) Central Aerological Observatory*, **64**.

Mcgraw, R. and Y. Liu, 2006: Brownian drift-diffusion model for evolution of droplet size distributions in turbulent clouds. *Geophys. Res. Lett.*, **33**, L03802.

Merkulovich, V. M. and A. S. Stepanov, 1981: Comments on the paper 'On the broadening of a droplet distribution by turbulence near cloud base' by M. J. Manton (Q. J. (1979),**105**,899-914). *Quart. J. R. Met. Soc.*, **107**, 976–977.

Politovich, M. K., 1993: A study of the broadening of droplet size distributions in cumuli. *J. Atmos. Sci.*, **50**, 2230–2244.

Politovich, M. K. and W. A. Cooper, 1988: Variability of the supersaturation in cumulus clouds. *J. Atmos. Sci.*, **45**, 1651–1664.

Pruppacher, H. R. and J. D. Klett, 1997: *Microphysics of Clouds and Precipitation*. Kluwer Academic, Boston, MA, USA, 2nd edition, 954 pp.

RAF, 2006a: Airborne measurements for cloud microphysics, RAF Bulletin No. 24., `http://www.eol.ucar.edu/raf/Bulletins`.

— 2006b: Standard output data products from the ncar research aviation facility, RAF Bulletin No. 9., `http://www.eol.ucar.edu/raf/Bulletins`.

Risken, H., 1989: *The Fokker-Planck Equation*. Springer-Verlag, Berlin, Heidelberg, New York, 2nd edition.

Rodts, S. M. A., P. G. Duynkerke, and H. J. J. Jonker, 2003: Size distributions and dynamical properties of shallow cumulus clouds from aircraft observations and satellite data. *J. Atmos. Sci.*, **60**, 1895–1912.

Sedunov, Y. S., 1965: Fine cloud structure and its role in the formation of the cloud particle spectrum. *Atmos. Ocean. Phys.*, **1**, 416–421.

Seminara, A., 2006: Personal communication.

Smirnov, V. I. and L. A. Nadeykina, 1986: On the theory of size spectrum of droplets formed by condensation in turbulent clouds. *Atmos. Ocean. Phys.*, **22**, 362–369.

Squires, P., 1952: The growth of cloud drops by condensation. 1. General characteristics. *Aust. J. Sci. Res.*, **A5**, 59–86.

Sutton, O. G., 1953: *Micrometeorology*. McGraw-Hill.

Vaillancourt, P. A., M. K. Yau, P. Bartello, and W. W. Grabowski, 2002: Microscopic approach to cloud droplet growth by condensation. Part II. turbulence, clustering, and condensational growth. *J. Atmos. Sci.*, **59**, 3421–3435.

Vaillancourt, P. A., M. K. Yau, and W. W. Grabowski, 2001: Microscopic approach to cloud droplet growth by condensation. Part I: Model description and results without turbulence. *J. Atmos. Sci.*, **58**, 1945–1964.

Voloshchuk, V. M. and Y. S. Sedunov, 1977: The kinetic equation of drop-spectrum evolution in the turbulent medium for the condensed stage in cloud development. *Sov. Meteor. Hydrol.*, **3**, 1–10.